

Design of lysine-free epidermal growth factor mutants for development of anti-cancer nanoconjugates

抗癌ナノコンジュゲートの開発のためのリジン欠損上皮成長因子変異体の設計

March, 2023

Aiwen ZHANG
张 爱文

Design of lysine-free epidermal growth factor mutants for development of anti-cancer nanoconjugates

抗癌ナノコンジュゲートの開発のためのリジン欠損上皮成長因子変異体の設計

March, 2023

Waseda University Graduate School of Advanced Science and Engineering

Department of Nanoscience and Nanoengineering, Research on Bioanalysis

Aiwen ZHANG

张 爱文

Table of contents

CHAPTER 1.....	8
GENERAL INTRODUCTION	8
1.1 CANCERS AND CANCER THERAPIES	8
1.2 EPIDERMAL GROWTH FACTOR RECEPTOR-TARGETED CANCER THERAPY	9
1.2.1 Monoclonal antibodies (mAbs)	10
1.2.2 Tyrosine kinase inhibitors (TKIs)	11
1.2.3 Disadvantage of the mAbs and TKIs in cancer treatment.....	11
1.2.4 Epidermal growth factor (EGF)-conjugated nanoparticles.....	12
1.2.4.1 Advantages of EGF-conjugated nanoparticles	13
1.3 STATEMENT OF THE PROBLEM	14
1.4 PROS AND CONS OF RECOMBINANT TECHNOLOGY	15
1.5 HYPOTHESIS AND AIM OF THIS STUDY	16
REFERENCE.....	17
CHAPTER 2.....	23
DESIGN AND PREPARATION OF THE LYSINE-FREE EPIDERMAL GROWTH FACTOR	
VARIANTS	23
2.1 SUMMARY	23
2.2 INTRODUCTION.....	23
2.3 MATERIALS AND METHODS.....	27
2.3.1 Cloning of mutant EGF without lysine site.....	27
2.3.2 Expression and purification of mutant EGF.....	28
2.3.3 Cell culture	29
2.3.4 ERK activity measurement.....	30
2.3.5 Binding activity assay by surface plasmon resonance (SPR).....	30

2.3.5.1 Preparation of EGFR-coated sensor chip	30
2.3.5.2 SPR measurements	32
2.3.6 Data analysis.....	32
2.4 RESULTS	33
2.4.1 Expression and verification of mutant EGF protein.....	33
2.4.1.1 Confirmation of the sequencing of the modified mutant EGF	33
2.4.1.2 Confirmation of the expressed products of EGF variants.....	34
2.4.2 Bioactivity of mutant EGF	35
2.4.3 Binding analysis of EGF variants by using SPR	37
2.5 DISCUSSION	39
2.6 CONCLUSION.....	41
REFERENCE.....	43
CHAPTER 3.....	47
CHARACTERIZATION OF MUTANT EGF-CONJUGATED GOLD NANOPARTICLES (GNPS)	47
3.1 SUMMARY	47
3.2 INTRODUCTION.....	48
3.3 MATERIALS AND METHODS.....	49
3.3.1 PEGylation of GNPs and chemical modification with EGF.....	49
3.3.2 Characterization of GNPs and EGF-GNPs.....	51
3.3.3 Cell culture	51
3.3.4 ERK activity measurement using cell ELISA.....	52
3.3.5 Binding Assay of EGF-GNPs.....	52
3.3.6 Evaluation of cell viability	53
3.3.7 Statistical analysis of the data	53
3.4 RESULTS	54
3.4.1 Conjugation of EGF with GNPs: preparation and characterization.....	54
3.4.2 Verification of bioactivity of EGF-GNPs.....	58
3.4.3 Binding analysis of EGF-GNPs.....	59

3.4.4 Effects of growth inhibition of EGF-GNPs on A431 cells	61
3.5 DISCUSSION	63
3.6 CONCLUSION	66
REFERENCE	67
CHAPTER 4.....	70
MECHANISTIC STUDY OF CYTOTOXIC INDUCTION BY EGF-GNP.....	70
4.1 SUMMARY	70
4.2 INTRODUCTION.....	70
4.3 MATERIALS AND METHODS.....	71
4.3.1 Materials and reagents.....	71
4.3.2 Cell culture	72
4.3.3 EGFR phosphorylation assay	72
4.3.4 Cellular uptake measurements	73
4.3.5 Immunofluorescence staining.....	74
4.3.6 Data analysis.....	75
4.4 RESULTS	75
4.4.1 Evaluation of EGFR phosphorylation of A431 cells	75
4.4.2 Cellular uptake of EGF-GNPs by A431 cells	77
4.4.3 EGFR and clathrin-coated vesicle colocalization analysis.....	78
4.5 DISCUSSION	80
4.6 CONCLUSION.....	83
REFERENCE.....	84
CHAPTER 5.....	86
CONCLUSIVE REMARKS AND PROSPECTS	86
5.1 CONCLUSIONS.....	86
5.2 FUTURE PERSPECTIVES	89
REFERENCE.....	90

ACKNOWLEDGMENT	91
LIST OF RESEARCH ACHIEVEMENTS	92

Table of Figures

Figure 1-1 The statistic of the disease and death caused by cancer.	9
Figure 1-2 The mechanism of EGFR targeted cancer therapy by using EGFR inhibitors.	12
Figure 1-3 Schematic illustrates the mechanism of EGF and EGF-GNP induced EGFR signaling activation and cell response.	14
Figure 1-4 The limitation of the current conjugation strategy.	15
Figure 2-1 Human EGF (PDB: 1JL9) and EGF/EGFR complex (PDB: 1IVO) three-dimensional structures, as well as wild type (WT) and mutant EGF amino acid sequences.	27
Figure 2-2 SPR schematic diagram (A) and representative sensorgram curve of SPR (B).	31
Figure 2-3 DNA sequencing for WT and mutant EGF.	34
Figure 2-4 EGF variants underwent SDS-PAGE analysis during purification.	35
Figure 2-5 The ERK phosphorylation of free EGF variants.	37
Figure 2-6 Immobilization of EGFR on the surface of the sensor chip: procedure and recorded sensorgram.	38
Figure 2-7 Analysis of the binding affinities of EGF variants.	39
Figure 3-1 Schematic diagram of the procedure for preparation of EGF-GNPs conjugates.	55
Figure 3-2 The quantified number of WT and EGF mutants immobilized to the nanoparticle.	56
Figure 3-3 UV-Vis spectrum of EGF-GNPs and PEG-GNPs.	57
Figure 3-4 Verification of the bioactivities of different kinds of EGF-GNPs.	59
Figure 3-5 Binding analysis of GNPs (without EGF) and EGF-GNPs.	61
Figure 3-6 Cell viability measurement after treatment with EGF-GNP conjugates.	63
Figure 4-1 Monitoring the state of EGFR phosphorylation using the EGFR	

phosphorylation array.....	76
Figure 4-2 Quantification of EGFR phosphorylation.....	77
Figure 4-3 Quantification of the cellular uptake of EGF-GNPs and GNPs.	78
Figure 4-4 Analysis of clathrin-EGFR colocalization after EGF-GNPs stimulation.	80
Figure 5-1 Illustration of the conclusion of this work.	88
Figure 5-2 Illustration of the possible application of mutant EGF.	90

Table of Tables

Table 1-1 The overexpression level of EGFR in different types of cancer.....	10
Table 2-1 The primer sequences that were utilized to create EGF mutants.....	28
Table 2-2 The kinetic rate parameters and derived dissociation constants of EGF variants.	39
Table 3-1 The polydispersity index (PDI) and hydrodynamic diameter of nanoparticles.....	57
Table 3-2 The zeta potential of functionalized GNP.	58

Chapter 1

General Introduction

1.1 Cancers and cancer therapies

There is a long history of cancer dating back to 3000 B.C. when it was first described and found in Edwin Smith Papyrus to illustrate breast cancer[1,2]. Over an extended period, cancer was considered an incurable disease until the surgery was developed and showed the effective ability to remove the tumor, especially for a tumor at an early stage[3]. However, it produces pain in the patients and shows low effectiveness for the tumor upon the occurrence of metastasis. With the discovery of X-rays by Roentgen in 1895, radiation therapy was developed and exhibited reasonable cure rates in cancer treatment[4,5]. This approach showed benefits in reducing pain for patients, but it caused side effects due to the non-selective killing of normal cells. Subsequently, in the 1930s, chemotherapy using chemical agents emerged in treating cancer, with remarkable results for curing cancer even in the advanced stage[6]. Until now, these strategies are still the primary modalities for cancer treatment, with successful reduction of morbidity and mortality of cancer overall to some extent[3,7]. However, from the statistical ratio of the disease and death caused by cancer, it remains the major problem that threatens people's health (Figure 1-1)[8]. That is because those approaches have not reduced mortality as much as we expected. Therefore, cancer research has been still conducted for decades to understand the properties of tumor cells and their formation mechanisms. One of the progresses among them is the discovery of the oncogenes that encode many receptor tyrosine kinases (RTKs). The RTKs play an

important role in various cellular processes and are often overexpressed in cancer cells[5,9]. Based on this, the advanced cancer therapy of “molecularly targeted cancer therapy” was developed by using drugs or substances to specifically target the RTKs to block their signaling and inhibit the spreading of the tumor[10–13]. This molecularly targeted cancer therapy significantly increased the selectivity of drugs to the cancer cells and reduces the side effects. It has aroused the enthusiasm of developing drugs or substances to target different RTKs.



Figure 1-1 The statistic of the disease and death caused by cancer. One in ten patients was caused by cancer, and one in six deaths was caused by cancer. The data was sourced from Institute for Health Metrics and Evaluation (IHME), Global Burden of Disease (2019).

1.2 Epidermal growth factor receptor-targeted cancer therapy

So far, there are fifty-eight RTK genes are known to exist in the human genome, and the transmembrane RTKs encoded by them are distributed in 20 subfamilies, such as epidermal growth factor receptor (EGFR), insulin receptor (InsR), platelet-derived growth factor receptor (PDGFR), vascular endothelial growth factor receptor (VEGFR), and hepatocyte growth factor receptor (HGFR)[14,15]. Among them, EGFR is the most well-studied and found as a major contributor to complex signaling in growth, migration, differentiation, and survival of cells[16–19]. Therefore, the abnormal activity of EGFR, through mutation or its overexpression, often results in tumor development[20,21]. In fact, EGFR overexpression has been found in many types of

tumors[22,23], such as head and neck, glioma, ovarian, colon, and rectum cancer, as shown in Table 1-1. Based on this, EGFR is the primary target for design in molecularly targeted agents and therapy. Until now, two types of agents have been mainly used in EGFR-targeted cancer therapy: monoclonal antibodies (mAbs) and tyrosine kinase inhibitors (TKIs). These two agents have different mechanisms to block the signaling of the EGFR[24].

Table 1-1 The overexpression level of EGFR in different types of cancer.

No.	Tumor type	Tumor overexpressing EGFR
1	Head and neck	80-90[25,26]
2	Cervical	6-90[27]
3	Non-small-cell lung cancer	40-89[28,29]
4	Glioblastoma	10-60[30,31]
5	Ovarian	35-75[32,33]
6	Pancreatic	30-50[34]
7	Colon and rectum	60-80[35]

1.2.1 Monoclonal antibodies (mAbs)

The mAbs (cetuximab, panitumumab) are large proteins with a molecular weight of around 150 kDa. These mAbs are explicitly designed to recognize the extracellular domain of EGFR at high binding affinity, whose dissociation constants are 0.1–0.2 nM and 0.05 nM for cetuximab and panitumumab, respectively[16]. Because of the high binding affinities, these mAbs can compete with endogenous ligands of EGFR and prevent the ligands from binding to the EGFR. This inhibits the activation of the

following intracellular signaling evoked by EGFR tyrosine kinase and eventually causes effective inhibition of cancer cell growth (Figure 1-2)[36–39]. Therefore, the results of clinical trials also showed reduced tumor progression and increased the survival rate of the patients.

1.2.2 Tyrosine kinase inhibitors (TKIs)

The TKIs, such as gefitinib, erlotinib, and canertinib, are synthetic chemicals with small size around 500 Da. Unlike mAbs, as shown in Figure 1-2, the TKIs bind to the intracellular catalytic domain of EGFR tyrosine kinase to compete with adenosine-5'-triphosphate (ATP). This prevents the ATP from binding to the EGFR, resulting in the blocking of autophosphorylation and activation of downstream signaling[36,37,40]. The TKIs applied in the cancer treatment also showed excellent anti-proliferative effects and increased survival rates of the patients in the clinical trial.

1.2.3 Disadvantage of the mAbs and TKIs in cancer treatment

Although these two strategies (mAbs and TKIs) of inhibition of EGFR have been approved for clinical use and have effective anti-cancer activity, the developed resistances with different mechanisms are the main challenge for the outcome of cancer treatment. Resistances to mAbs are mainly caused by the mutation of EGFR, activation of alternative signaling, altered VEGF/VEGFR expression, and epithelial-mesenchymal transition[41,42]. To overcome the reduced anti-cancer effect, the dosage of mAbs needs to be increased. For TKIs, there are also several mechanisms of the development of resistances, such as oncogenic shift, bypass signal activation, and the secondary EGFR mutation, resulting in the escape of the cancer cells and increased survival. Therefore, it is necessary to develop a new modality that targets EGFR but uses alternative mechanisms to reduce resistance to cancer treatment.

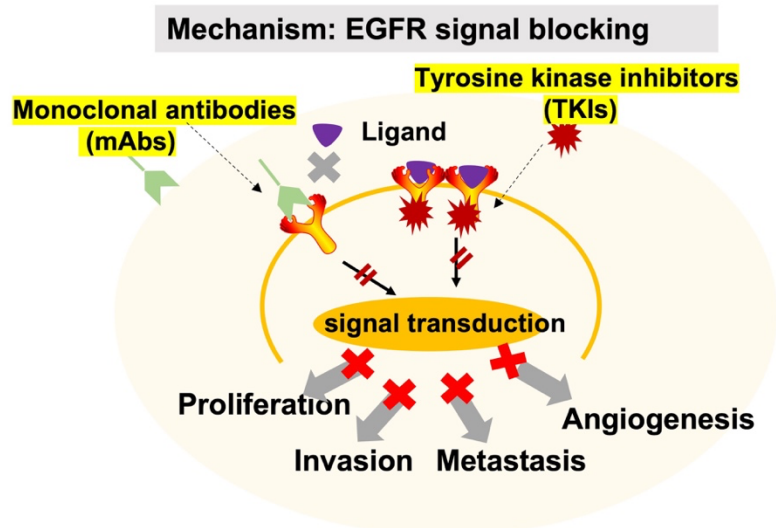


Figure 1-2 The mechanism of EGFR targeted cancer therapy by using EGFR inhibitors. The mAbs and TKI are the common EGFR inhibitors that specially bind to the EGFR, resulting in EGFR signaling blocking. mAbs: monoclonal antibodies; TKIs: tyrosine kinase inhibitors.

1.2.4 Epidermal growth factor (EGF)-conjugated nanoparticles

Recently, it has been identified that the EGF-conjugated nanoparticles (NPs) have a unique aspect that exhibits tumor cytotoxicity by activating rather than blocking the signaling of the EGFR[43]. The EGF is a small natural ligand of the EGFR with a 6 kDa molecular weight[44]. It is surprising to see the anticancer effect with the EGF-NPs considering that the conjugated natural ligand has an opposite effect on EGFR from the above-mentioned mAbs and TKIs. In fact, both soluble EGF and EGF-NPs activate EGFR and following signaling; nevertheless, the final outcomes are different (Figure 1-3). More specifically, soluble EGF induces cell proliferation, differentiation, and migration[45], whereas EGF-NPs causes the death of tumor cells through apoptosis[43,46]. The plausible mechanism of this EGF-NPs induced death of cancer cells is supposed to be the sustained activation of EGFR signaling in the endosomes of the cells, which is caused by the multivalency of the EGF conjugated to the NPs and can be influenced by the size of the NPs and density of the EGF[46,47]. As a result of

conjugating to gold nanoparticles (GNPs), which results from the alternated interaction of the EGF-EGFR and state of EGFR at the membrane, it has also been discovered that lipid rafts play a crucial role in the activity conversion of EGF from its initial anti-apoptotic to pro-apoptotic state[43].

1.2.4.1 Advantages of EGF-conjugated nanoparticles

Even though the exact mechanism of cellular responses to EGF-NPs has not been clarified completely, there are three major advantages of EGF-conjugated nanoparticles in anti-cancer agents over mAbs and TKIs. Firstly, the mechanism of EGF-conjugated NPs induced cell death differs from EGFR inhibitors, which utilize the activation of EGFR signaling. This altered mechanism could reduce many types of resistance caused by altered growth factor expression and mutations of the sites in the kinase domain of the EGFR. Apart from this, a recent study has found that EGFR functions differently in primary and metastatic tumors, acting as a driver of the primary tumor and suppressor of the metastatic tumor[48]. This finding indicates that the inhibition of EGFR activation dominated by mAbs and TKIs is not beneficial for the treatment of metastatic tumors. Conversely, EGF, as one of the EGFR agonists, that modulate EGFR agonism may be helpful in the treatment of metastatic tumors. In addition, an early work in our group found that the EGF-NPs can significantly induce apoptosis in the cancer cell with high expression of the EGFR; for normal cells that also overexpressed EGFR, the apoptosis induction of EGF-NPs is minimum, indicating the selective apoptosis induction in EGFR overexpressed cancer cells[49].

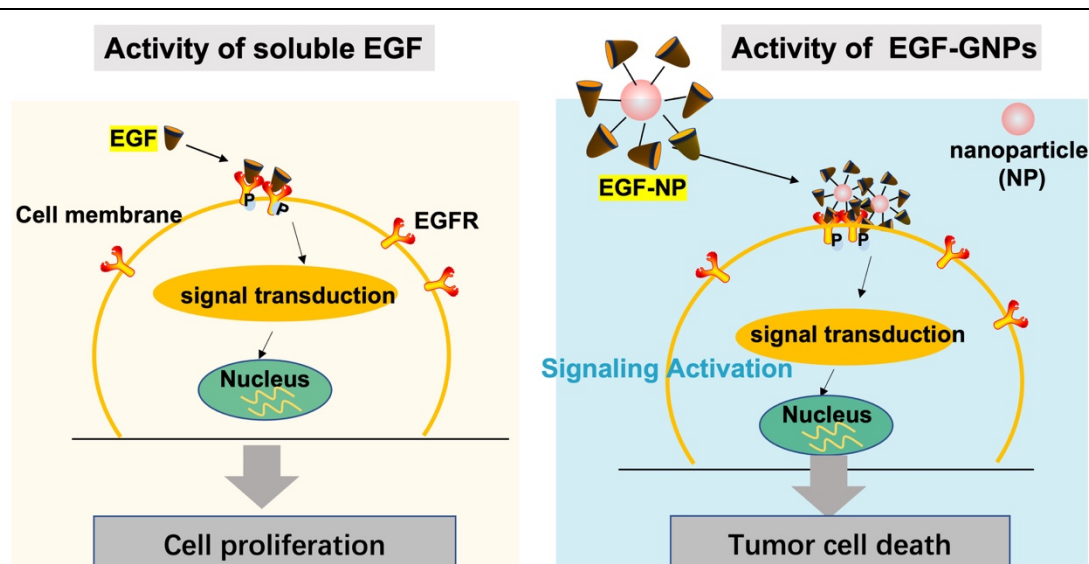


Figure 1-3 Schematic illustrates the mechanism of EGF and EGF-GNP induced EGFR signaling activation and cell response. Upon binding to the EGFR, both EGF and EGF-GNP activate the signaling of EGFR but can induce different cell responses.

1.3 Statement of the Problem

According to the potential advantages of EGF-conjugated NPs, the EGF-conjugated gold nanoparticles (EGF-GNPs) have been studied by several groups due to their easy functionalization of gold nanoparticles (GNPs). However, these studies demonstrated that the EGF-GNPs did not show high activity as expected. Given the promise of EGF-conjugated NPs, improving its efficiency in applying this new modality to clinical use is necessary. One likely interpretation for the poor activity of EGF-NPs is the present conjugation method, as illustrated in Figure 1-4, in which EGF molecules are conjugated to the surface of NPs in random orientations due to the various reactive functional groups existing in EGF. If this is the case, EGF molecules, which are bound in inappropriate orientations, become unfavorable to interact with EGFR, thereby reducing the overall activity of EGF-NPs. If the EGF can be conjugated to the NP in a specific orientation, which is favorable for the interaction with EGFR (Figure 1-4, middle), all of the EGF molecules immobilized on the nanoparticle would be more likely to engage with EGFR, increasing the activity of EGF-NPs. To achieve this, one of the straightforward approaches is to create new EGF mutants with only a

single group that can react with nanoparticles.

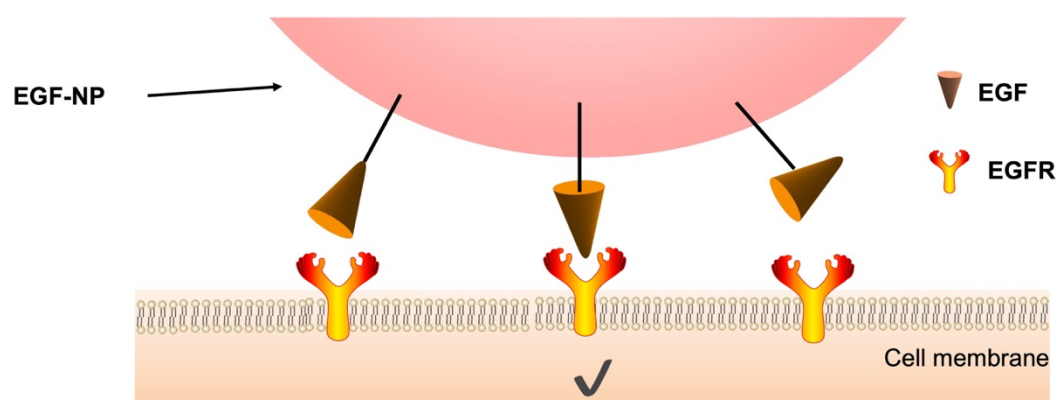


Figure 1-4 The limitation of the current conjugation strategy. As shown from it, the EGF, which conjugated to the nanoparticle by chemical coupling, presented a different orientation on the surface of the NP.

1.4 Pros and cons of recombinant technology

Protein engineering techniques, such as site-directed mutagenesis, directed evolution, and random mutagenesis, are powerful for modifying the protein to obtain the single functional group of it. It is well-documented in many applications that site-specific conjugation of the protein to the materials results in an improved activity than that of the randomly conjugated protein[50–52]. However, there is also a drawback in potentially altering the bioactivity and binding affinity of the protein after mutagenesis, eventually influencing the activity of protein conjugates, as well. Given this consideration, most studies verify the protein mutants whether retain their bioactivity and binding affinity to their receptors. For instance, Yamamoto et al. constructed six clones of TNF- α , which do not have lysine residues to limit the reactive amino group to the N-terminal one. In this study, they could select only one mutant which showed similar binding affinity and bioactivity to the wild-type protein[53]. Thus selected mutant exhibited higher bioactivity, upon conjugated to polyethylene glycol (PEG) site-selectively, than the randomly conjugated wild-type TNF- α [53]. Similarly, Narimatsu et al. selected a mutant cytokine lymphotoxin- α with a single functional group, which

has identical bioactivity to the wild-type lymphotoxin- α [54]. Compared with PEGylated wild-type lymphotoxin- α , the mutant that allowed site-specific modification achieved improved anti-tumor activity[54].

On the other hand, as I discussed in the previous sections, the reaction of EGF-GNP is different from that of normal soluble EGF, and their responsive mechanism is still not clarified completely. In this regard, there will be not only a negative effect (lowering intrinsic activity) but also a positive effect by mutation to boost the cytotoxic activities of mutant EGF-GNP conjugates against tumor cells. Therefore, there are two possibilities, namely the orientation control and positive effect of mutation on the intrinsic EGF activity, to enhance the activity of EGF-GNPs

1.5 Hypothesis and aim of this study

On the basis of this idea and those discussed in the previous sections, in this dissertation, I hypothesized that the lysine-free EGF mutants would allow me to elucidate the design rationale for the development of a more potent EGF-GNP as an anti-cancer agent. To examine this hypothesis, I designed new lysine-free EGF mutants and studied the activity upon conjugation to GNP. This dissertation has achieved the following: 1) designing and developing new lysine-free EGF mutants which have comparable activities to that of wild-type EGF, 2) conjugation of the lysine-free EGF to the NP and evaluation of the activity of the EGF-GNPs to EGFR in vitro and in a cancer cell line, 3) mechanism investigation of the mutant EGF-NP-induced selective cytotoxicity to the cancer cells.

Reference

- 1 Hajdu, S. I. (2011) A note from history: Landmarks in history of cancer, part 1. *Cancer* **117**, 1097–1102.
- 2 Di Lonardo, A., Nasi, S. and Pulciani, S. (2015) Cancer: We should not forget the past. *J. Cancer* **6**, 29–39.
- 3 Wu, H., Chang, D. and Huang, C. (2006) Targeted Therapy for Cancer. *J. Cancer Mol.* **2**, 57–66.
- 4 Mould, R. F. (1995) Röntgen and the discovery of X-rays. *Br. J. Radiol.* **68**, 1145–1176.
- 5 Baskar, R., Lee, K. A., Yeo, R. and Yeoh, K. W. (2012) Cancer and radiation therapy: Current advances and future directions. *Int. J. Med. Sci.* **9**, 193–199.
- 6 Arruebo, M., Vilaboa, N., Sáez-Gutierrez, B., Lambea, J., Tres, A., Valladares, M. and González-Fernández, Á. (2011) Assessment of the evolution of cancer treatment therapies. *Cancers (Basel)*. **3**, 3279–3330.
- 7 Najafi, M., Majidpoor, J., Toolee, H. and Mortezaee, K. (2021) The current knowledge concerning solid cancer and therapy. *J. Biochem. Mol. Toxicol.* **35**, e22900.
- 8 Global Burden of Disease Collaborative Network. Global Burden of Disease Study 2019 (GBD 2019) Reference Life Table. Seattle, United States of America: Institute for Health Metrics and Evaluation (IHME). 2021.
- 9 Blume-Jensen, P. and Hunter, T. (2001) Oncogenic kinase signalling. *Nature* **411**, 355–365.
- 10 Debela, D. T., Muzazu, S. G., Heraro, K. D., Ndalama, M. T., Mesele, B. W., Haile, D. C., Kitui, S. K. and Manyazewal, T. (2021) New approaches and procedures for cancer treatment: Current perspectives. *SAGE Open Med.* **9**, No. 20503121211034366.
- 11 Lee, Y. T., Tan, Y. J. and Oon, C. E. (2018) Molecular targeted therapy: Treating

-
- cancer with specificity. *Eur. J. Pharmacol.* **834**, 188–196.
- 12 Gerber, D. E. (2008) Targeted therapies: A new generation of cancer treatments. *Am. Fam. Physician* **77**, 311–319.
- 13 Kim, J. A. (2003) Targeted therapies for the treatment of cancer. *Am. J. Surg.* **186**, 264–268.
- 14 Bhullar, K. S., Lagarón, N. O., McGowan, E. M., Parmar, I., Jha, A., Hubbard, B. P. and Rupasinghe, H. P. V. (2018) Kinase-targeted cancer therapies: Progress, challenges and future directions. *Mol. Cancer* **17**, 1–20.
- 15 Lemmon, M. A. and Schlessinger, J. (2011) Cell signaling by receptor-tyrosine kinases. *Cell* **141**, 1117–1134.
- 16 Santos, E. D. S., Nogueira, K. A. B., Fernandes, L. C. C., Martins, J. R. P., Reis, A. V. F., Neto, J. D. B. V., Júnior, I. J. D. S., Pessoa, C., Petrilli, R. and Eloy, J. O. (2021) EGFR targeting for cancer therapy: Pharmacology and immunoconjugates with drugs and nanoparticles. *Int. J. Pharm.* **592**, 120082.
- 17 Seshacharyulu, P., Ponnusamy, M. P., Haridas, D., Jain, M., Ganti, A. K. and Batra, S. K. (2012) Targeting the EGFR signaling pathway in cancer therapy. *Expert Opin. Ther. Targets* **16**, 15–31.
- 18 Du, Z. and Lovly, C. M. (2018) Mechanisms of receptor tyrosine kinase activation in cancer. *Mol. Cancer* **17**, 1–13.
- 19 London, M. and Gallo, E. (2020) Epidermal growth factor receptor (EGFR) involvement in epithelial-derived cancers and its current antibody-based immunotherapies. *Cell Biol. Int.* **44**, 1267–1282.
- 20 Sigismund, S., Avanzato, D. and Lanzetti, L. (2018) Emerging functions of the EGFR in cancer. *Mol. Oncol.* **12**, 3–20.
- 21 Voldborg, B. R., Damstrup, L., Spang-Thomsen, M. and Poulsen, H. S. (1997) Epidermal growth factor receptor (EGFR) and EGFR mutations, function and possible role in clinical trials. *Ann. Oncol.* **8**, 1197–1206.
- 22 Thomas, R. and Weihua, Z. (2019) Rethink of EGFR in cancer with its kinase

-
- independent function on board. *Front. Oncol.* **9**, 1–16.
- 23 Mitsudomi, T. and Yatabe, Y. (2010) Epidermal growth factor receptor in relation to tumor development: EGFR gene and cancer. *FEBS J.* **277**, 301–308.
- 24 Dassonville, O., Bozec, A., Fischel, J. L. and Milano, G. (2007) EGFR targeting therapies: Monoclonal antibodies versus tyrosine kinase inhibitors. Similarities and differences. *Crit. Rev. Oncol. Hematol.* **62**, 53–61.
- 25 Ang, K. K., Andratschke, N. H. and Milas, L. (2004) Epidermal growth factor receptor and response of head-and-neck carcinoma to therapy. *Int. J. Radiat. Oncol. Biol. Phys.* **58**, 959–965.
- 26 Kalyankrishna, S. and Grandis, J. R. (2006) Epidermal Growth Factor Receptor Biology in Head and Neck Cancer. *J. Clin. Oncol.* **24**, 2666–2672.
- 27 Soonthornthum, T., Arias-pulido, H., Joste, N., Lomo, L., Muller, C., Rutledge, T. and Verschraegen, C. (2011) Epidermal growth factor receptor as a biomarker for cervical cancer. *Ann. Oncol.* **22**, 2166–2178.
- 28 Prabhakar, C. N. (2015) Epidermal growth factor receptor in non-small cell lung cancer. *Transl. Lung Cancer Res.* **4**, 110–118.
- 29 Lynch, T. J., Bell, D. W., Sordella, R., Gurubhagavatula, S., Okimoto, R. A., Brannigan, B. W., Harris, P. L., Haserlat, S. M., Supko, J. G., Haluska, F. G., et al. (2004) Activating Mutations in the Epidermal Growth Factor Receptor Underlying Responsiveness of Non–Small-Cell Lung Cancer to Gefitinib. *N. Engl. J. Med.* **350**, 2129–39.
- 30 Hatanpaa, K. J., Burma, S., Zhao, D. and Habib, A. A. (2010) Epidermal growth factor receptor in glioma: Signal transduction, neuropathology, imaging, and radioresistance. *Neoplasia* **12**, 675–684.
- 31 Xu, H., Zong, H., Ma, C., Ming, X., Shang, M., Li, K., He, X., Du, H. and Cao, L. (2017) Epidermal growth factor receptor in glioblastoma (Review). *Oncol. Lett.* **14**, 512–516.
- 32 Salomon, D. S., Brandt, R., Ciardiello, F. and Normanno, N. (1995) Epidermal

-
- growth factor-related peptides and their receptors in human malignancies. *Crit. Rev. Oncol. Hematol.* **19**, 183–232.
- 33 Bartlett, J. M., Langdon, S. P., Simpson, B. J., Stewart, M., Katsaros, D., Sismondi, P., Love, S., Scott, W. N., Williams, A. R., Lessells, A. M., et al. (1996) The prognostic value of epidermal growth factor receptor mRNA expression in primary ovarian cancer. *Br. J. Cancer, England* **73**, 301–306.
- 34 Bloomston, M., Bhardwaj, A., Ellison, E. C. and Frankel, W. L. (2006) Epidermal Growth Factor Receptor Expression in Pancreatic Carcinoma Using Tissue Microarray Technique. *Dig. Surg.* **23**, 74–79.
- 35 Pabla, B., Bissonnette, M. and Konda, V. J. (2015) Colon cancer and the epidermal growth factor receptor: Current treatment paradigms, the importance of diet, and the role of chemoprevention. *World J Clin Oncol* **6**, 133–142.
- 36 Yewale, C., Baradia, D., Vhora, I., Patil, S. and Misra, A. (2013) Epidermal growth factor receptor targeting in cancer: A review of trends and strategies. *Biomaterials* **34**, 8690–8707.
- 37 Yamaoka, T., Ohba, M. and Ohmori, T. (2017) Molecular-targeted therapies for epidermal growth factor receptor and its resistance mechanisms. *Int. J. Mol. Sci.* **18**, 2420.
- 38 Li, S., Schmitz, K. R., Jeffrey, P. D., Wiltzius, J. J. W., Kussie, P. and Ferguson, K. M. (2005) Structural basis for inhibition of the epidermal growth factor receptor by cetuximab. *Cancer Cell* **7**, 301–311.
- 39 Gravalos, C., Cassinello, J., García-Alfonso, P. and Jimeno, A. (2010) Integration of panitumumab into the treatment of colorectal cancer. *Crit. Rev. Oncol. Hematol.* **74**, 16–26.
- 40 Pytel, D., Sliwinski, T., Poplawski, T., Ferriola, D. and Majsterek, I. (2009) Tyrosine Kinase Blockers: New Hope for Successful Cancer Therapy. *Anticancer. Agents Med. Chem.* **9**, 66–76.
- 41 Hopper-Borge, E. A., Nasto, R. E., Ratushny, V., Weiner, L. M., Golemis, E. A.

-
- and Astsaturov, I. (2009) Mechanisms of tumor resistance to EGFR-targeted therapies. *Expert Opin. Ther. Targets* **13**, 339–362.
- 42 Wheeler, D. L., Dunn, E. F. and Harari, P. M. (2010) Understanding resistance to EGFR inhibitors-impact on future treatment strategies. *Nat. Rev. Clin. Oncol.* **7**, 493–507.
- 43 Yamamoto, S., Iwamaru, Y., Shimizu, Y., Ueda, Y., Sato, M., Yamaguchi, K. and Nakanishi, J. (2019) Epidermal growth factor-nanoparticle conjugates change the activity from anti-apoptotic to pro-apoptotic at membrane rafts. *Acta Biomater.* **88**, 383–391.
- 44 Carpenter, G. and Cohen, S. (1990) Epidermal growth factor. *J. Biol. Chem.* **265**, 7709–7712.
- 45 Wong, R. W. C. and Guillaud, L. (2004) The role of epidermal growth factor and its receptors in mammalian CNS. *Cytokine Growth Factor Rev.* **15**, 147–156.
- 46 Wu, L., Xu, F. and Reinhard, B. M. (2016) Nanoconjugation prolongs endosomal signaling of the epidermal growth factor receptor and enhances apoptosis. *Nanoscale* **8**, 13755–13768.
- 47 Yasami-Khiabani, S., Karkhaneh, A., Shokrgozar, M. A., Amanzadeh, A. and Golkar, M. (2020) Size effect of human epidermal growth factor-conjugated polystyrene particles on cell proliferation. *Biomater. Sci.* **8**, 4832–4840.
- 48 Ali, R. and Wendt, M. K. (2017) The paradoxical functions of EGFR during breast cancer progression. *Signal Transduct. Target. Ther.* **2**, 16042.
- 49 Yamamoto, S. and Nakanishi, J. (2021) Epidermal growth nanoparticle conjugates-induced cellular responses : Effect of interfacial parameters between cell and nanoparticle. *Anal. Sci.* **37**, 741–745.
- 50 Morishige, T., Yoshioka, Y., Narimatsu, S., Ikemizu, S., Tsunoda, S. ichi, Tsutsumi, Y., Mukai, Y., Okada, N. and Nakagawa, S. (2013) Mutants of lymphotoxin- α with augmented cytotoxic activity via TNFR1 for use in cancer therapy. *Cytokine* **61**, 578–584.

-
- 51 Morishige, T., Yoshioka, Y., Inakura, H., Tanabe, A., Yao, X., Tsunoda, S. ichi, Tsutsumi, Y., Mukai, Y., Okada, N. and Nakagawa, S. (2010) Creation of a lysine-deficient LIGHT mutant with the capacity for site-specific PEGylation and low affinity for a decoy receptor. *Biochem. Biophys. Res. Commun.* **393**, 888–893.
- 52 Bach, M., Hölig, P., Schlosser, E., Völkel, T., Graser, A., Müller, R. and Kontermann, R. E. (2003) Isolation from phage display libraries of lysine-deficient human epidermal growth factor variants for directional conjugation as targeting ligands. *Protein Eng.* **16**, 1107–1113.
- 53 Yamamoto, Y., Tsutsumi, Y., Yoshioka, Y., Nishibata, T., Kobayashi, K., Okamoto, T., Mukai, Y., Shimizu, T., Nakagawa, S., Nagata, S., et al. (2003) Site-specific pegylation of a lysine-deficient TNF- α with full bioactivity. *Nat. Biotechnol.* **21**, 546–552.
- 54 Narimatsu, S., Yoshioka, Y., Watanabe, H., Masano, T., Morishige, T., Yao, X., Tanabe, A., Tsunoda, S. ichi, Tsutsumi, Y., Mukai, Y., et al. (2011) Lysine-deficient lymphotoxin- α mutant for site-specific PEGylation. *Cytokine* **56**, 489–493.

Chapter 2

Design and preparation of the lysine-free epidermal growth factor variants

2.1 Summary

Epidermal growth factor (EGF), which is vital for cellular activities, is frequently coupled with biomaterials for wide-ranging applications. However, due to the multiple endogenous reactive functional groups existing in the EGF molecule, the activity of the conjugated EGF can be deviated by the heterogeneous orientation of EGF to the material. Therefore, there were various challenges in earlier work to control the orientation of EGF on materials without drastically altering its original activities. Herein, in this chapter, I designed two new lysine-free EGF variants (K28S/K48R (SR); K28R/K48S (RS)), in which the lysine was replaced by serine (S) or arginine (R), restricting the reactive site to the N-terminus. The activities of them (SR and RS), in terms of EGF receptor (EGFR) binding and phosphorylation of extracellular signal-regulated kinase (ERK), were comparable or slightly increased from those of wild-type (WT) EGF, confirming the EGF mutants retain or rather improve the capability to bind to the EGFR and activate the intracellular signaling. Therefore, they are suitable for the development of more potent EGF-GNPs, which this thesis addresses.

2.2 Introduction

The epidermal growth factor (EGF), is a protein with a molecular weight of 6 kDa, composed of 53 amino acids, and was first isolated from the submandibular gland of

mice[1,2]. Subsequently, it was found in many tissues, such as the placenta and kidney, as well as from different species[2]. It has been identified as one of the members of growth factors that activate EGF receptor (EGFR)[3]. The binding of EGF to EGFR first induces dimerization of EGFR and initiates the activation of tyrosine kinase. The activity of EGFR is also controlled by the trafficking of the EGF-EGFR complex via internalization and degradation in the cell[4]. Through these complex processes, EGF can regulate various cellular processes, such as migration, differentiation, proliferation, and survival[2].

Due to the important role of EGF in cellular processes mentioned above, there has been intense interest in the use of EGF in many biomaterials, such as nanoparticles (NPs)[5], polyethylene glycol (PEG)[6,7], and scaffolds[8], for improved efficiency in imaging[9], cancer diagnosis[10], targeted drug delivery[11], cancer therapy[12], and tissue engineering[13]. Especially, EGF is often used as a potent targeting moiety to improve the delivery efficiency to cancer cells that overexpress EGFR[14,15]. However, the steric hindrance of biomaterials can significantly prevent the conjugated EGF molecule from binding to the cell-surface receptor, which can lower its binding as well as functional activities[16,17]. Therefore, many researchers made efforts to control the orientation of EGF to the materials for fully exploiting its activity by site-specific conjugation. In this regard, controlling the coupling condition is one of the common strategies to achieve site-specific conjugation of EGF to biomaterials. For example, Lee et al. reported, at an acidic pH condition ($\text{pH} = 5.5$), most EGF molecules were conjugated to PEG at the N-terminal; the conjugates showed high activity than the randomly conjugated EGF[18]. However, the acidic condition also reduces the coupling efficiency of the EGF to the material. Alternatively, several studies were conducted to utilize the mouse EGF, which does not have endogenous lysine residues in its sequence, thereby the conjugation site is confined to the N-terminal of EGF when the amide coupling was used for the reaction[19]. However, it was anticipated that the mouse EGF can induce immune responses when applied in the human body since there is only 70%

of homoeology between mouse EGF and human EGF[11]. Therefore, this strategy is not suitable specifically for biomedical applications. In addition, it has been reported that the binding affinity of mouse EGF is three times lower than that of human EGF[1].

As an alternative strategy, the site-directed chemical coupling of EGF to biomaterials can be achieved by genetic recombinant technology. In this strategy, all the reactive amino acid residues, except for the desired one, were replaced with non-reactive amino acids to limit the conjugation site at the single residue[20]. Within endogenous reactive functional groups, such as amino, carboxy, and thiol groups, commonly used for chemical coupling, the number of the amino group is the least in EGF; there is only three residues existed in EGF at lysine 28, lysine 48, and N-terminus. Therefore, mutating the two lysines is enough to limit the conjugation site to N-terminus. This is a good choice for minimizing the potential modification of the biological activities of EGF by mutation. In addition, since several studies showed the N-terminus is good for bioconjugation,[6,21] developing the lysine-free EGF variants is the suitable strategy for my purpose, that is to develop more active EGF-GNP conjugates.

To design the lysine-free EGF, other amino acids should be introduced in place of lysine residues. However, as shown from the crystal structure of EGF-EGFR (Figure 2-1A, B), two lysine residues on EGF are located close to the important residues, which is essential for the interaction of EGF and EGFR. Therefore, if inappropriate residues are introduced there, the interaction between EGF and EGFR will be disturbed. Thereby, the choice of alternative amino acids is crucial. To choose the amino acids, I first investigated the sequences from other species (Figure 2-1C). As shown from it, lysines in the wild-type EGF can be replaced by serine (S) or arginine (R). Meanwhile, Bach et al. used a phage-display library to look for lysine-free EGF variants[11]. This study identified multiple mutants, where K28 and K48 were replaced with other residues without drastically influencing its binding activity EGFR. Especially, one EGF mutant

(K28Q/R45S/K48S/R53S) has been shown to exhibit comparable binding activity to the WT EGF. Given this, it seems that the mutation of K48S does not influence the binding activity to EGFR. In addition, Campion et al. reported an EGF mutant (K28R) that had a slightly increased binding affinity for EGFR compared to WT[22]. However, another study found that the mutant EGF with both lysines replaced with R revealed decreased activity compared with wild-type one[23]. Based on these earlier studies and sequences investigated, I designed two new original mutants of EGF (K28R/K48S (RS)) and SR(K28S/K48R).

Based on the above consideration, in this chapter, I created the RS and SR mutants as lysine-free EGF as the basis for the development of EGF-GNPs in the following chapters. The cDNA sequences of EGF mutants were generated by using site-directed mutagenesis. The *E. coli* Origami 2 (DE3) was used to express the EGF mutants. Their purity and expression of the mutant EGF products were confirmed. Finally, the activities of the EGF variants, in terms of ERK phosphorylation and binding ability, were investigated.

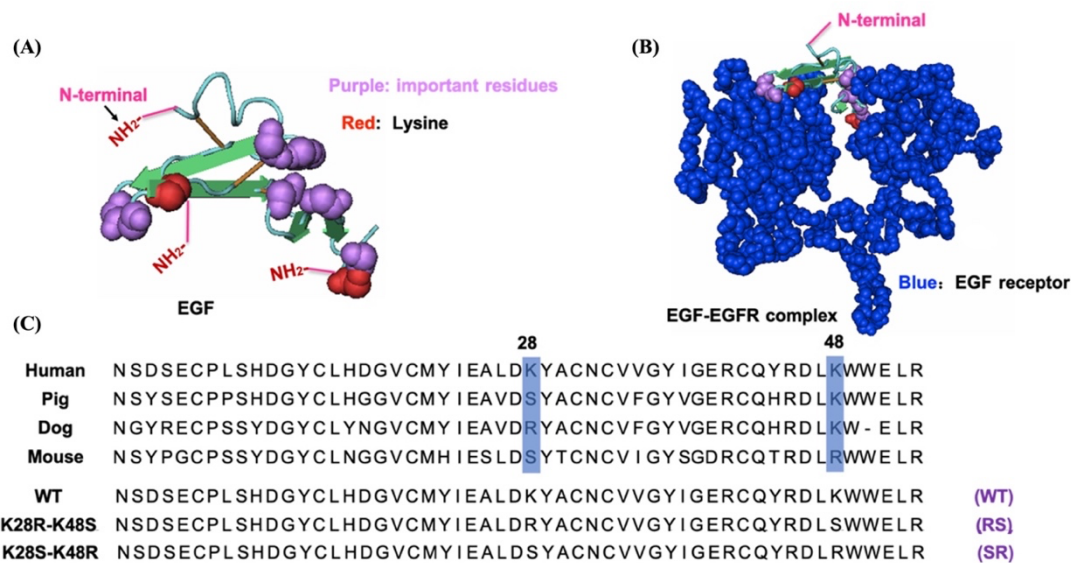


Figure 2-1 Human EGF (PDB: 1JL9) and EGF/EGFR complex (PDB: 1IVO) three-dimensional structures, as well as wild type (WT) and mutant EGF amino acid sequences. (A) The 3D structure of Human EGF. Lysine residues and important residues are represented by the colors red and purple, respectively. (B) The EGF-EGFR complex structure. The EGFR is depicted in blue in the space-fill model. (C) Sequential alignments of EGF from different species and designed mutant EGF. Blue boxes highlight the residues 28 and 48, which correspond to two lysins in human EGF. In the designed mutants EGF, two lysine residues of WT EGF were replaced with either arginine or serine. Adapted from Ref. [24], <https://doi.org/10.1080/14686996.2021.1944783>, under the terms of the CC BY license.

2.3 Materials and Methods

2.3.1 Cloning of mutant EGF without lysine site

Polymerase chain reaction (PCR) was used to create the cDNA sequences of wild-type (WT) and mutant EGF using the appropriate primers listed in Table 2-1. First, by using oligohistidine-tagged human EGF (hEGF-His₆)[25] as a template, the cDNA sequence of WT EGF was amplified by using a set of primers (P1 and P2, Sigma-Aldrich, MO, USA) via polymerase chain reaction (PCR). The P1 primer contains the cDNA sequence of the C-terminal region of glutathione-S-transferase (GST) and the N-terminal region of EGF. On the other hand, the P2 primer contains the Not I site and the C-terminal region of EGF. Next, the glutathione-S-transferase (GST)-tagged WT

EGF sequence was amplified by the PCR reaction using the mega-primer created from the reverse sequence of the above PCR product and the T7 promoter (TAATACGACTCACTATAG, Sigma-Aldrich) against pET-41a as a template, and then subcloned into the XbaI/NotI site of pET-41a (Merck, Darmstadt, Germany). In this way, the thrombin cleavage site cDNA sequence was inserted between the EGF sequence and the GST-tag. The cDNA of mutant EGF was created from WT EGF by PCR using the primer pairs P1 and P3 (Sigma-Aldrich) for RS, and P1 and P4 (Sigma-Aldrich) for SR.

Table 2-1 The primer sequences that were utilized to create EGF mutants. Lowercase red letters are used to indicate the codons that relate to the mutation locations.

P1	5'-	GCGGGTCTGGTGCCACGCGGATCCAATAGTGAATGTCC
P2	5'-	CCCGCGGCCGCTAGCGCAGTTCACCACTT
P3	5'-	CCCGCGGCCGCTAGCGCAGTTCACCAggaCAGGTCTCGGTACTGACATCGCTCCC CGATGTAGCCAACAACACAGTTGCATGCATctGTCCAATGCTTCAATATAC
P4	5'-	CCCGCGGCCGCTAGCGCAGTTCACCActCAGGTCTCGGTACTGACATCGCTCCC CGATGTAGCCAACAACACAGTTGCATGCATggaGTCCAATGCTTCAATATAC

Adapted from Ref. [24], <https://doi.org/10.1080/14686996.2021.1944783>, under the terms of the CC BY license.

2.3.2 Expression and purification of mutant EGF

E. coli Origami 2. (DE3) (EMD Millipore, MA, USA) was transformed by the pET-41a vector harboring the GST-hEGF fusion construct. Then, the transformed cells were added to the LB culture medium, which contained kanamycin (Wako, Osaka, Japan), and inoculated at 37°C overnight. The next day, at 37°C on a shaker, the cultivated cells were added and allowed to scale up to 500 mL of LB media containing kanamycin. After that, isopropyl-β-D-thiogalactopyranoside (IPTG, Wako) was added to stimulate protein expression, when the turbidity of the culture medium at 600 nm (OD600) reached around 0.6. The collected and pelleted cells were then lysed in a

benzonase-containing BugBuster protein extraction reagent (EMD Millipore). The supernatant was mixed with the glutathione Sepharose beads (GE-healthcare, IL, USA). The lysate and GS beads were combined and then added to the column for washing with ice-cold thrombin-digestion buffer. The GS beads were then transferred to a tube containing thrombin digestion buffer together with biotinylated thrombin. The mixture was centrifuged after an overnight reaction, and the supernatant was then gathered. The avidin-agarose resin was then added, and the mixture was then stirred at 4°C for 30 minutes. After a short centrifugation, the supernatant containing EGF protein was put into a new tube. Thus, using Any kD™ Mini-Protein® TGX™ gels (Bio-Rad, CA, USA), sodium dodecyl sulfate polyacrylamide electrophoresis (SDS-PAGE) was used to analyze WT and mutant EGF. The direct enzyme-linked immunosorbent assay (ELISA) method, mentioned in the prior study[12], was used to measure the hEGF concentration. Briefly, the 96-well plate was coated with EGF overnight, then washed and blocked for an hour with 1% bovine serum albumin (BSA, Wako) before being incubated with rabbit anti-human EGF antibody (Abcam, Cambridge, UK) and anti-rabbit IgG horseradish peroxidase (Sigma-Aldrich). Finally, a micro-plate reader (Bio-Rad) was used to measure the signal at 450 nm following the addition of 3,3',5,5'-Tetramethylbenzidine (TMB, Sigma-Aldrich) substrate.

2.3.3 Cell culture

A431 cells (RCB0202), which a model cancer line, were acquired from the RIKEN cell bank (Ibaraki, Japan) and grown at 37°C in a humidified environment containing 5% CO₂ in Dulbecco's Modified Eagle's Medium (DMEM, Sigma-Aldrich) supplemented with 1% penicillin-streptomycin (Wako, Osaka, Japan) and 10% fetal bovine serum (FBS, BioWest, Nuaille, France)

2.3.4 ERK activity measurement

A431 cells were grown at a density of 20,000 cells per well in a 96-well plate overnight. Following that, the medium was replaced with 50 μ L of media devoid of FBS to serum-starve the cells for 4 h. Cells were treated with different samples (DMEM and free EGF with different concentrations). After 5 min reaction, the solution in the well was removed, and the cells were rinsed with PBS before being exposed to 150 μ L of 4% paraformaldehyde in PBS for 20 minutes at room temperature. The cells were permeabilized with 150 μ L of 0.5% Triton X-100 (Sigma-Aldrich) in PBS after being washed three times with PBS. After 20 min incubation, the cells were blocked for 1 hour with 2% BSA in PBS. Then, rabbit monoclonal antibodies against phospho-ERK1/2 (T202/Y204) (Cell Signaling Technology, MA, USA) were added to each well at a volume of 50 μ L for 2h. A further round of washing was followed by the addition of 100 μ L of anti-rabbit IgG alkaline phosphatase (Sigma-Aldrich) (1:3000). The cells were then rinsed once again, and 100 μ L of 4-nitrophenyl phosphate disodium salt hexahydrate (Sigma-Aldrich) was added as a substrate. The signal was obtained at 405 nm using the microplate reader.

2.3.5 Binding activity assay by surface plasmon resonance (SPR)

2.3.5.1 Preparation of EGFR-coated sensor chip

Here, the surface plasmon resonance (SPR), a biosensor technique used to study the interactions of biomolecules by keeping track of changes in the refractive index from the sensor chip and recording them in the sensorgram, was employed to quantify the binding activity of the EGF mutants. For instance, as seen in Figure 2-2B, when a sample is injected, the analyte inside it can be collected by the ligand that is coated on the sensor chip, increasing the signal of the binding response, which is referred to as

the association phase. The collected analyte may dissociate when the buffer containing no analyte was supplied, decreasing the binding response. This process is known as dissociation. During this process, the kinetics of analyte-ligand binding can be calculated using certain equations. In view of this, in this experiment, hEGFR should be immobilized on the surface of the sensor chip first.

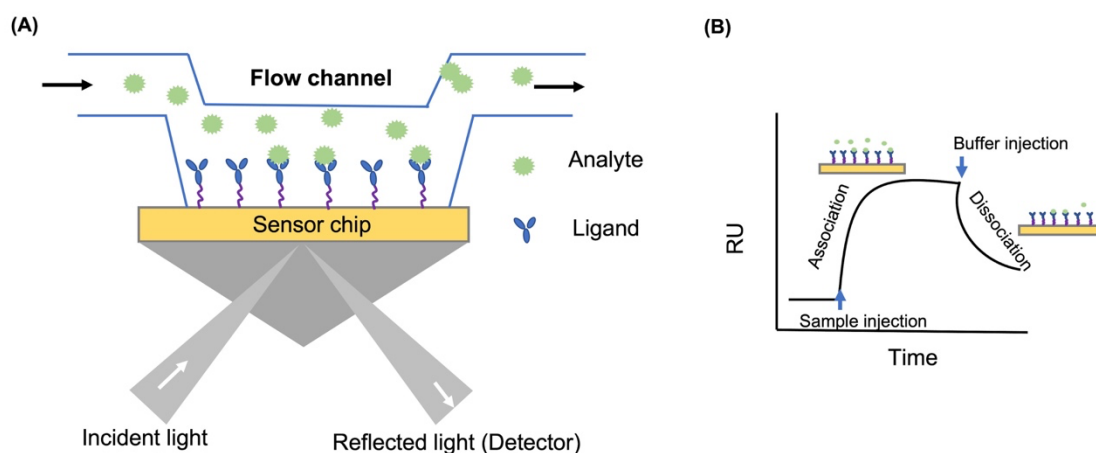


Figure 2-2 SPR schematic diagram (A) and representative sensorgram curve of SPR (B). RU: response units.

Here, the CM5 sensor chip (GE Healthcare), a gold-coated sensor chip with carboxymethylated dextran covalently bonded to its surface, was used for immobilization due to its low nonspecific absorbance compared to other types of sensor chips. The procedure is as follows. Briefly, the recombinant human EGFR extracellular domain (hEGFR, Sigma-Aldrich, MO, USA) was immobilized on the CM5 sensor chip via amine coupling. First, a 1:1 solution of 0.4 M 1-ethyl-3-(3-dimethylaminopropyl) carbodiimide (EDC, GE healthcare) and 0.1 M N-hydroxy succinimide (NHS, GE healthcare) was added at a rate of 10 $\mu\text{L}/\text{min}$ for 7 minutes to activate the carboxy group of the dextran matrix on the sensor device. The hEGFR was then reacted with the activated surface at a concentration of 10 $\mu\text{g}/\text{mL}$ in 10 mM sodium acetate (GE healthcare) (pH 4.5) at a rate of 5 $\mu\text{L}/\text{min}$ until the desired immobilization level at 2000 response units (RU) was reached. Finally, 1 M ethanolamine-HCl (GE healthcare,) (pH 8.5) at 10 $\mu\text{L}/\text{min}$ for 7 min was injected to block the uncoupled sites of the active

carboxy group on the sensor chip.

2.3.5.2 SPR measurements

The X100 instrument (Biacore Life Science, Uppsala, Sweden) was used for the SPR tests. At 25°C in a degassed HBS-EP running buffer (GE Healthcare, Illinois, USA), the soluble EGF (WT, SR, and RS) binding experiment was carried out. EGF was flowed over the hEGFR-immobilized sensor chip at different concentrations (1.6, 6.3, 25, 100, and 400 nM) at a rate of 30 µL/min for 2 min. Between each injection, HBS-EP buffer was applied at a rate of 30 µL/min for 1 min to renew the surface of the sensor chip.

The sensorgram can be used to track the mass change on the surface of the sensor chip in real time as well as the change in refractive index. The program BIAEvaluation was used to examine the sensorgrams (Biacore Life Sciences). Fitting the sensorgrams with a 1:1 Langmuir binding model yielded the kinetic parameters (on rate and off rate) of each EGF variant (Equation 1). The equilibrium dissociation constant (K_D) of EGF was determined by the ratio of on rate (k_{on}) and off rate (k_{off}) by following equations:



$$\frac{d[\text{EGFR}][\text{EGF}]}{dt} = k_a * [\text{EGFR}][\text{EGF}] - k_d * [\text{EGF} \cdot \text{EGFR}] \quad (2)$$

$$\frac{d[\text{EGF} \cdot \text{EGFR}]}{dt} = -k_d * [\text{EGF} \cdot \text{EGFR}] \quad (3)$$

In the formula (1), the forward reaction rate was k_a and the reversed reaction rate was defined as k_d .

2.3.6 Data analysis

A two-tailed F -test was used to calculate the variances of the results under the null hypothesis of equal variance. After that, a two-tailed student t -test was employed to ascertain whether each group's results were statistically significant. A P -value of 0.05

or less was considered statistically significant.

2.4 Results

2.4.1 Expression and verification of mutant EGF protein

2.4.1.1 Confirmation of the sequencing of the modified mutant EGF

Following the PCR procedure, a pET-41a vector carrying the GST-thrombin tag sequence was used to clone the plasmid DNA generating EGF with a single NH₂ group. To confirm the presence of the desired modification, the DNA sample of mutant EGF was sent out for the sequencing. Figure 2-3 shows the sequencing of the designed DNA of EGF variants (WT, SR, and RS). As shown from it, the original codons of WT at lysine sites were AAG. After modification, for the SR and RS, the codons at these two sites were replaced by AGA and TCC, respectively, which confirmed the substitution of the lysine with serine (S) or arginine (R).



Figure 2-3 DNA sequencing for WT and mutant EGF. The altered nucleotides were highlighted by red rectangle lines on the DNA sequencing maps for the SR and RS mutants.

2.4.1.2 Confirmation of the expressed products of EGF variants

After confirmation of the successful modification of the DNA sequences for the EGF variants, the plasmids were used for the expression of the mutant EGF proteins. The extraction and purification process were confirmed by SDS-PAGE (Figure 2-4A). Even though the GST-tagged EGF was not detected in the total lysate (Figure 2-4A, lane 2), its enrichment can be confirmed upon reacting the lysate with the GST resin (Figure 2-4A, lane 4, ~36 kDa). Following digestion by biotinylated thrombin, it was split into EGF and GST, which can be identified as 6 and 26 kDa bands, respectively

(Figure 2-4A, lane 5). After separating the remaining thrombin, the different EGF mutants were effectively obtained with the right size of 6 kDa (Figure 2-4A, lane 6). All the EGF variants, namely WT, SR, and RS, bands were detected found in lanes 8, 9, and 10, respectively, as illustrated in Figure 2-4B. The EGF band was the only band that can be seen in these lanes, demonstrating the excellent purity of the produced protein.

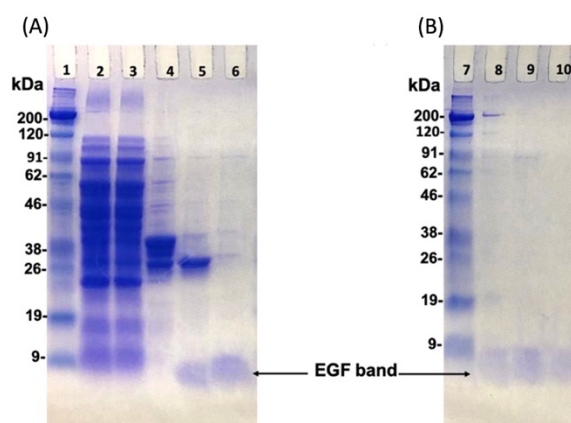


Figure 2-4 EGF variants underwent SDS-PAGE analysis during purification. The Coomassie Brilliant Blue was used to stain polyacrylamide gels. Lane 1 and 7: protein makers. Lane 2: the total protein in the supernatant of cell lysate. Lane 3: the unbound protein after GS resin adsorption. Lane 4: the eluted protein from GS resin by using SDS-loading buffer. Lane 5: the eluted protein by the digestion of thrombin. Lane 6: the purified WT EGF after biotin-avidin separation. Following the final biotin-avidin purification, the WT, SR, and RS are compared in lanes 8, 9, and 10. The bands of EGF protein were denoted by arrows. Adapted from Ref. [24], <https://doi.org/10.1080/14686996.2021.1944783>, under the terms of the CC BY license.

2.4.2 Bioactivity of mutant EGF

Here, I utilized an enzyme-linked immunosorbent assay (ELISA)[26], to assess the biological activity of the EGF mutant by focusing on the phosphorylation of extracellular signal-regulated kinase (ERK) in A431 cells that overexpressed EGFR. When EGF binds to the EGFR, ERK is activated and phosphorylated, followed by delivering mitogen signals to intracellular destinations[27]. The level of phosphorylated ERK is a good predictor of the bioactivity of mutant EGF in the cell sample[14]. Figure

2-5 depicts the changes in relative ERK phosphorylation levels after different concentrations of mutant EGF and WT EGF being applied to the cells. As the concentration was increased, both the EGF mutants and the WT resulted in dose-dependent increases in the amount of ERK phosphorylation. Between the 10 ng/mL and 100 ng/mL groups, the ERK phosphorylation did not seem to rise noticeably after treating by WT and RS, likely because the response was approaching saturation. On the other hand, there was a slight difference between these two concentrations for the SR. However, when I further analyzed the ERK phosphorylation at a further higher concentration (1000 ng/mL, Figure 2-5 insert), there was no difference compared with 100 ng/mL. The results confirmed that the ERK phosphorylation had been saturated at 100 ng/mL. In earlier work from our group, EGK phosphorylated saturated in a similar fashion[12]. Therefore, it was reasonable to see ERK activity saturation in this concentration range. Of note, there was a slightly lower activity of the SR at 1 ng/mL, but it could be complemented by increasing the concentration, whereas the activity at saturation concentration represented its capability to activate EGFR and more essential for the application. Given this, when I looked at the maximum responses of the RS and SR mutants, they exhibited comparable levels of phosphorylation to that of WT EGF. Therefore, I can conclude that the two mutants showed similar activity as WT EGF.

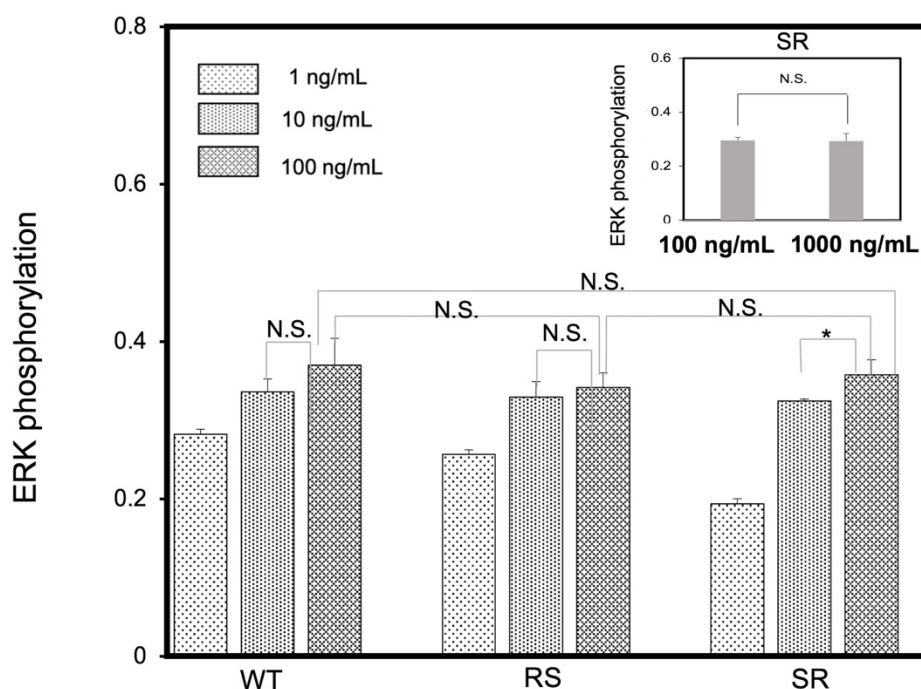


Figure 2-5 The ERK phosphorylation of free EGF variants. Each EGF variant (WT, SR, and RS) was added to A431 cells with different concentration (1 ng, 10 ng, and 100 ng/mL) for 5 min. ERK phosphorylation levels were then measured using an in-situ cell ELISA. The inserted image represents the ERK phosphorylation levels in A431 cells treated with high concentrations of SR (100 and 1000 ng/mL). Mean \pm SD was obtained from three independent experiments. *: $P < 0.05$. Adapted from Ref. [24], <https://doi.org/10.1080/14686996.2021.1944783>, under the terms of the CC BY license.

2.4.3 Binding analysis of EGF variants by using SPR

Next, the SPR was used to direct evaluation of the interaction between EGF and EGFR in a pure system, which is a potent technique for analyzing molecular interactions that are widely used in biology[28]. Since the natural EGFR is a membrane protein and is not soluble in aqueous solutions. Therefore, in place of native EGFR, I utilized the commercial extracellular domain of recombinant human EGFR, which includes the EGF binding sites. By utilizing amine coupling, EGFR was immobilized on a CM5 sensor chip with a carboxymethylated dextran matrix (Figure 2-6A). In Figure 2-6B, the sensorgram was displayed. It recorded the real-time response throughout every stage of immobilization. From that, the application of EGFR led to

an increase in the baseline after EDC/NHS being activated the carboxy group on the sensor chip. The EGFR solution was continually injected until the EGFR molecule was successfully immobilized at 2000 resonance units (RU) (Figure 2-6B). The 2000 RU setting is calculated by the following formula: $\text{immobilized EGFR (RU)} = (\text{MW}_{\text{EGF}} / \text{MW}_{\text{EGFR}}) \times \text{Stoichiometry} / R_{\text{max}}$, to ensure a specific binding. About 2000 pg/mm² of coated EGFR was present on the sensor chip since 1 RU was approximately equal to 1 pg/mm² of the immobilized protein. Throughout the entirety of the EGF binding experiment, this EGFR mass density on the sensor chip remained constant.

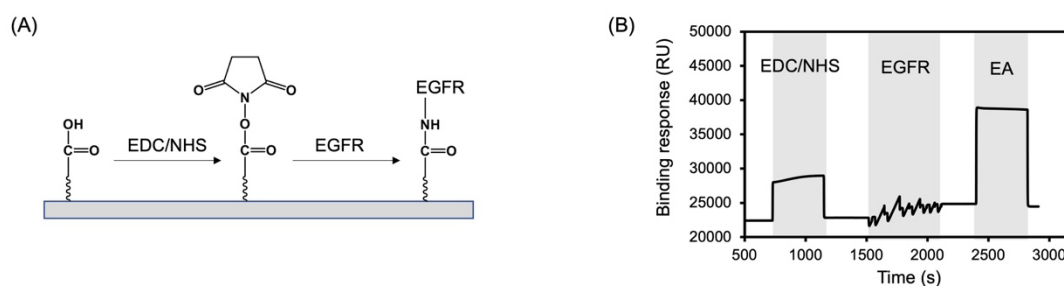


Figure 2-6 Immobilization of EGFR on the surface of the sensor chip: procedure and recorded sensorgram. (A) Diagram of the amine coupling process was utilized to immobilize the sensor chip using EGFR. (B) Real-time monitoring of SPR sensorgram during immobilization of EGFR on a sensor chip. The mixture of EDC/NHS was injected for 420 s to activate the surface of the CM5 sensor chip. Next, EGFR was injected until the desired immobilization at 2000 RU was attained. Finally, the ethanolamine (EA) was injected for 420s to block the remaining active carboxy group on the sensor chip. Reproduced from Ref. [29] with permission from Springer Nature, Copyright [2023].

Then, the EGF variants with different concentrations were flowed over the EGFR-coated sensor chip, followed by its dissociation with the buffer solution. The changes in the binding response were recorded and used for calculating the binding characteristics of the EGF variants to EGFR. Figure 2-7 displays the dose-dependent binding responses for WT EGF (A) and EGF mutants (B, SR; C, RS). After analyzing the sensorgrams, the quantified dissociation constant (K_D), which was derived from the dissociation rate (k_{off}) and association rate (k_{on}) can be obtained (Table 2-2). The results demonstrated that the dissociation constants of SR and WT were similar (55.2 ± 5.2 nM and 55.0 ± 4.0 nM, respectively), but the dissociation constant of RS was lower (37.5

$\pm 3.2 \text{ nM} < 55.0 \text{ nM}$), indicating that RS bound to EGFR more strongly than WT and SR. It concluded that the designed EGF mutants (SR and RS) did not lose their ability to bind to the EGFR. Also, the slight increase in the binding constants for RS indicated that there might be some beneficial effects for their activities in EGF-GNPs.

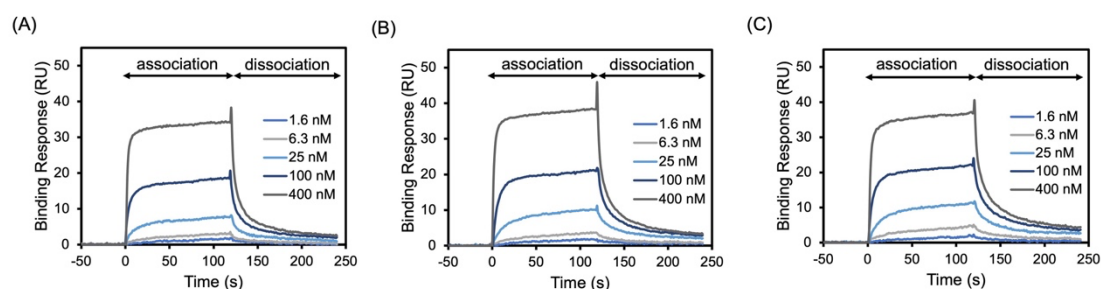


Figure 2-7 Analysis of the binding affinities of EGF variants. Sensorgrams from the WT (A), SR (B), and RS (C) with phases of association and dissociation phases. A series concentration (from 400 to 1.6 nM, with 4 times dilution) of EGF solution was introduced over the EGFR-coated sensor for 2 min before being dissociated by buffer for another 2 min. Reproduced from Ref. [29] with permission from Springer Nature, Copyright [2023].

Table 2-2 The kinetic rate parameters and derived dissociation constants of EGF variants.

	WT	SR	RS
$K_D \text{ (nM)}^*$	55.0 ± 4.0	55.2 ± 5.2	37.5 ± 3.2
$k_{on} \text{ (1/M} \cdot \text{s)} \times 10^{5**}$	4.4 ± 0.2	4.7 ± 0.2	5.5 ± 0.3
$k_{off} \text{ (1/s)} \times 10^{-3**}$	24.3 ± 1.2	25.9 ± 1.8	20.5 ± 0.7

* The off-rate (k_{off}) and on-rate (k_{on}) were generated from the sensorgrams by using equations described in the experimental section. The data reflects the mean and standard deviation of triplicates.

* The following formula was used to calculate the dissociation constant (K_D): $K_D = k_{on}/k_{off}$.

* Adapted from Ref. [29] with permission from Springer Nature, Copyright [2023].

2.5 Discussion

In this work, after preliminary literature-based investigation and homologous substitution from other species, two EGF variants (RS and SR) without lysine residues were designed and prepared. The changed sequencing of DNA molecules of EGF

mutants compared with WT EGF, indicating the successful modification of the DNA molecules (Figure 2-3). Thereby, the *E. coli* expression system was chosen for the synthesis of mutant EGF proteins due to its simplicity, fast growth, and flexibility to various vectors[30]. However, there are several strains in this system, such as *E. coli* Origami(DE3), *E. coli* BL21 (DE3), and *E. coli* DH5 α , with different intracellular environments leading to various characteristics of expressed proteins[31]. In this work, I first tried the *E. coli* BL21 (DE3). However, the degradation of the expressed protein was observed, which might be due to the misfolding of the EGF. Given this, the *E. coli* Origami(DE3) was selected as the host cell to express the EGF protein, since several studies reported it facilitates the formation of disulfide bonds and increases the solubility of the proteins[31,32], which are also key problems in the recombinant protein production. In addition, GST was used to fusion the expression of proteins of EGF to further increase the stability of the expressed protein[33]. After analysis by SDS-PAGE, the GST-tagged EGF, which was seen as about 36 kDa on the gel (Figure 2-4A, lane 4), confirmed the high expression and solubility of produced EGF, indicating the GST fusion partner and *E. coli* Origami (E3) were suitable for producing EGF. Furthermore, the thrombin was used to digest the GST tag to release the EGF. It should be noted that this process was conducted under mild conditions which was beneficial for the production of the EGF when compared with other chemical treatment[34]. Finally, the products of the EGF proteins were confirmed with high purity, indicating the multiple steps of purification were really worked (Figure 2-4B), which can be used for the biological assay without inferences from other components. The results shown above supported the methods utilized to create the EGF proteins and can be used as a reference for future research on the development and manufacturing of different recombinant EGF proteins.

Despite the fact that the EGF mutant protein had been successfully generated, its activity still needed to be verified. The majority of earlier investigations on the assessment of EGF mutants have concentrated on the binding affinity of EGF to EGFR,

which was thought to regulate the biological activity of EGF. The relationship between binding affinity and biological activity, however, is not always consistent. Given this, in this work, both binding affinity and bioactivity of the EGF variant were evaluated. The ERK, which is a signal molecule belonging to the essential signaling cascade, mitogen-activated protein kinase (MAPK), is considered as a downstream phosphorylation marker to evaluate the full bioactivity of the EGF[18,35]. Figure 2-5 confirmed the saturated concentration for the ERK phosphorylation of the EGF variants was at 100 ng/mL. Furthermore, the WT and mutant EGF (SR and RS) exhibited similar activities at this concentration, demonstrating that the developed EGF mutants, in which lysine residues were substituted with serine or arginine, did not affect their ability to trigger the signaling of the EGFR. Following, the binding affinity of EGF were obtained by the SPR assay. Table 2-2 shows quantified dissociation constant of EGF variants. From that, the binding activity of WT and SR were almost same. Meanwhile, it was suprising that the RS had higher binding activity than them. It is noteworthy that the lysine 48 of EGF is located close to the EGF-EGFR binding interface and that the mutation of the positively charged residue into serine (S) lowers the charge of that region. This change might be preferable for the interaction of EGF-EGFR and the reason for the increased binding affinity for the RS. Combination of the activity of binding and ERK phosphorylation, the lysine-free EGF were successfully developed without losing the original activities, indicating the strategy of selection of the substituted residues could be useful, and the lysine-free EGF mutants can be used for the following studies of the NP conjugates.

2.6 Conclusion

In this work, I constructed lysine-free recombinant EGF mutants by replacing two inherent lysine residues with either serine (S) or arginine (R) to obtain a single amino group at N-terminal of EGF for optimization of the bioconjugation. With careful design, the lysine-free EGF mutants were successful prepared with high purity. After

verification of the activity, in term of the activation of the EGFR signaling and ability to interaction with EGFR, the mutants EGF retained the comparable activities or slightly higher activity with WT EGF, which was promising to be used as an orientation-controlled ligands conjugated NPs for improving the activity of the conjugates.

Reference

- 1 Nexø, E. and Frede Hansen, H. (1985) Binding of epidermal growth factor from man, rat and mouse to the human epidermal growth factor receptor. *Biochim. Biophys. Acta - Gen. Subj.* **843**, 101–106.
- 2 Zeng, F. and Harris, R. C. (2014) Epidermal growth factor, from gene organization to bedside. *Semin. Cell Dev. Biol.* **28**, 2–11.
- 3 Lahti, J. L., Lui, B. H., Beck, S. E., Lee, S. S., Ly, D. P., Longaker, M. T., Yang, G. P. and Cochran, J. R. (2011) Engineered epidermal growth factor mutants with faster binding on-rates correlate with enhanced receptor activation. *FEBS Lett.* **585**, 1135–1139.
- 4 Barbieri, M. A., Roberts, R. L., Gumusboga, A., Highfield, H., Alvarez-Dominguez, C., Wells, A. and Stahl, P. D. (2000) Epidermal growth factor and membrane trafficking: EGF receptor activation of endocytosis requires Rab5a. *J. Cell Biol.* **151**, 539–550.
- 5 Yasami-Khiabani, S., Karkhaneh, A., Shokrgozar, M. A., Amanzadeh, A. and Golkar, M. (2020) Size effect of human epidermal growth factor-conjugated polystyrene particles on cell proliferation. *Biomater. Sci.* **8**, 4832–4840.
- 6 Lee, H. and Park, T. G. (2002) Preparation and characterization of mono-PEGylated epidermal growth factor: Evaluation of in vitro biologic activity. *Pharm. Res.* **19**, 845–851.
- 7 Kim, T. H., Lee, H. and Park, T. G. (2002) Pegylated recombinant human epidermal growth factor (rhEGF) for sustained release from biodegradable PLGA microspheres. *Biomaterials* **23**, 2311–2317.
- 8 Bavaro, T., Tengattini, S., Rezwan, R., Chiesa, E., Temporini, C., Dorati, R., Massolini, G., Conti, B., Ubiali, D. and Terreni, M. (2021) Design of epidermal growth factor immobilization on 3D biocompatible scaffolds to promote tissue repair and regeneration. *Sci. Rep.* **11**, 1–13.

-
- 9 Yuan, Q., Lee, E., Yeudall, W. A. and Yang, H. (2010) Dendrimer-triglycine-EGF nanoparticles for tumor imaging and targeted nucleic acid and drug delivery. *Oral Oncol.* **46**, 698–704.
 - 10 Ryu, J. H., Shin, M., Kim, S. A., Lee, S., Kim, H., Koo, H., Kim, B. S., Song, H. K., Kim, S. H., Choi, K., et al. (2013) In vivo fluorescence imaging for cancer diagnosis using receptor-targeted epidermal growth factor-based nanoprobe. *Biomaterials* **34**, 9149–9159.
 - 11 Bach, M., Hölig, P., Schlosser, E., Völkel, T., Graser, A., Müller, R. and Kontermann, R. E. (2003) Isolation from phage display libraries of lysine-deficient human epidermal growth factor variants for directional conjugation as targeting ligands. *Protein Eng.* **16**, 1107–1113.
 - 12 Yamamoto, S., Iwamaru, Y., Shimizu, Y., Ueda, Y., Sato, M., Yamaguchi, K. and Nakanishi, J. (2019) Epidermal growth factor-nanoparticle conjugates change the activity from anti-apoptotic to pro-apoptotic at membrane rafts. *Acta Biomater.* **88**, 383–391.
 - 13 Masters, K. S. (2011) Covalent growth factor immobilization strategies for tissue repair and regeneration. *Macromol. Biosci.* **11**, 1149–1163.
 - 14 Kim, W., Na, K.-Y., Lee, K.-H., Lee, H. W., Lee, J. K. and Kim, K.-T. (2017) Selective uptake of epidermal growth factor-conjugated gold nanoparticle (EGF-GNP) facilitates non-thermal plasma (NTP)-mediated cell death. *Sci. Rep.* **7**, 10971.
 - 15 Wu, P., Zhou, Q., Zhu, H., Zhuang, Y. and Bao, J. (2020) Enhanced antitumor efficacy on coloncancer using EGF functionalized PLGA nanoparticles loaded with 5-Fluorouracil and perfluorocarbon. *BMC Cancer* **20**, 354.
 - 16 Boucher, C., St-Laurent, G., Loignon, M., Jolicœur, M., De Crescenzo, G. and Durocher, Y. (2008) The bioactivity and receptor affinity of recombinant tagged EGF designed for tissue engineering applications is defined by the nature and position of the tags. *Tissue Eng. - Part A* **14**, 2069–2077.

-
- 17 Coates, D. R., Chin, J. M. and Chung, S. T. L. (2014) Designing Protein-Based Biomaterials for Medical Applications. *Acta Biomater* **10**, 1542–1557.
- 18 Haeshin Lee, Il Ho Jang, Sung Ho Ryu, and T. G. P. (2003) N-Terminal Site-Specific Mono-PEGylation of Epidermal Growth Factor. *Entomol. Exp. Appl.* **20**, 818–825.
- 19 Carlsson, J., Blomquist, E., Gedda, L., Liljegren, Å., Malmström, P. U., Sjöström, A., Sundin, A., Westlin, J. E., Zhao, Q., Tolmachev, V., et al. (1999) Conjugate chemistry and cellular processing of EGF-dextran. *Acta Oncol. (Madr)*. **38**, 313–321.
- 20 Khan, S., Ullah, M. W., Siddique, R., Nabi, G., Manan, S., Yousaf, M. and Hou, H. (2016) Role of recombinant DNA technology to improve life. *Int. J. Genomics* **2016**.
- 21 Yamamoto, Y., Tsutsumi, Y., Yoshioka, Y., Nishibata, T., Kobayashi, K., Okamoto, T., Mukai, Y., Shimizu, T., Nakagawa, S., Nagata, S., et al. (2003) Site-specific pegylation of a lysine-deficient TNF- α with full bioactivity. *Nat. Biotechnol.* **21**, 546–552.
- 22 Niyogi, S. K., Campion, S. R. and Tadaki, D. K. (1992) Evaluation of the role of electrostatic residues in human epidermal growth factor by site-directed mutagenesis and chemical modification. *J. Cell. Biochem.* **50**, 35–42.
- 23 Bachran, C., Schneider, S., Riese, S. B., Bachran, D., Urban, R., Schellmann, N., Zahn, C., Sutherland, M. and Fuchs, H. (2011) A lysine-free mutant of epidermal growth factor as targeting moiety of a targeted toxin. *Life Sci.* **88**, 226–232.
- 24 Zhang, A. and Nakanishi, J. (2021) Improved anti-cancer effect of epidermal growth factor-gold nanoparticle conjugates by protein orientation through site-specific mutagenesis. *Sci. Technol. Adv. Mater.* **22**, 616–626.
- 25 Kato, K., Sato, H. and Iwata, H. (2005) Immobilization of Histidine-Tagged Recombinant Proteins onto Micropatterned Surfaces for Cell-Based Functional Assays. *Langmuir* **21**, 7071–7075.

-
- 26 Crowther, J. R. (2009) The ELISA guidebook. Second., Humana press, New York, NY, USA.
- 27 Patel, A. L. and Shvartsman, S. Y. (2018) Outstanding questions in developmental ERK signaling. *Dev.* **145**, dev143818.
- 28 Nguyen, H. H., Park, J., Kang, S. and Kim, M. (2015) Surface plasmon resonance: A versatile technique for biosensor applications. *Sensors (Switzerland)* **15**, 10481–10510.
- 29 Zhang, A., Abdellatef, S. A. and Nakanishi, J. (2023) Mechanistic investigation into selective cytotoxic activities of gold nanoparticles functionalized with epidermal growth factor variants. *Anal. Sci.* **39**, 395–405.
- 30 Rosano, G. L. and Ceccarelli, E. A. (2014) Recombinant protein expression in *Escherichia coli*: Advances and challenges. *Front. Microbiol.* **5**, 172.
- 31 Li, D., Ji, F., Huang, C. and Jia, L. (2019) High expression achievement of active and robust Anti- β 2 microglobulin Nanobodies via *E.coli* Hosts Selection. *Molecules* **24**, 2860.
- 32 Xiong, S., Wang, Y. F., Ren, X. R., Li, B., Zhang, M. Y., Luo, Y., Zhang, L., Xie, Q. L. and Su, K. Y. (2005) Solubility of disulfide-bonded proteins in the cytoplasm of *Escherichia coli* and its “oxidizing” mutant. *World J. Gastroenterol.* **11**, 1077–1082.
- 33 Sakhel, B., Jayanthi, S., Muhoza, D., Okoto, P., Krishnaswamy Suresh Kumar, T. and Adams, P. (2021) Simplification of the purification of heat stable recombinant low molecular weight proteins and peptides from GST-fusion products. *J. Chromatogr. B* **1172**, 122627.
- 34 Waugh, D. S. (2011) An overview of enzymatic reagents for the removal of affinity tags. *Protein Expr. Purif.* **80**, 283–293.
- 35 Keel, B. A. and Davis, J. S. (1999) Epidermal growth factor activates extracellular signal-regulated protein kinases (ERK) in freshly isolated porcine granulosa cells. *Steroids* **64**, 654–658.

Chapter 3

Characterization of mutant EGF-conjugated gold nanoparticles (GNPs)

3.1 Summary

Epidermal growth factor-nanoparticles (EGF-NPs) are an appealing new therapeutic modality for the treatment of cancers that overexpress EGF receptors (EGFR). However, the insufficient cytotoxicity of the random orientation of the EGF to GNPs might be the main problem for cytotoxic induction of the EGF-GNPs. Site-specific conjugation of EGF molecules to GNPs by using mutants with a single functional group is a promising method for changing the activity of EGF-GNPs. Thereby, the lysine-free EGF mutants, which I developed in the last chapter, were used to obtain the site-specifically conjugated EGF-GNPs. The results demonstrated the different activities of the various EGF-GNPs. Especially one mutant EGF showed increased activities in terms of interaction with EGFR, EGFR signaling activation, and cytotoxic induction to the cancer cells compared with random conjugated EGF-GNPs in wild-type EGF. However, another EGF mutant only showed similar cytotoxicity to the wild-type EGF-GNPs. Since the lysine-free EGF mutants retained full activities, the induced different cytotoxicity of EGF-GNPs indicated the synergistic effect of both orientation and intrinsic properties of the mutants.

3.2 Introduction

As an alternative to conventional EGFR-targeted agents, EGF-NP is considered a potential anti-cancer agent that targets EGFR but exhibits tumor cytotoxicity by different mechanisms. Despite its potential, the insufficient cytotoxic activity of EGF-NP hampered its translation to the next step in drug development. Based on this idea, in the last chapter, two lysine-free EGF mutants, namely SR (K28S/K48R) and RS (K28R/K48S), which have only a single primary amino group at the *N*-terminus, were successfully created, aiming to limit the conjugation site and orientation control on NP. The activities of these two lysine-free EGF were comparable, or even higher binding activity for RS, compared to wild-type EGF (WT). Since previous studies demonstrated that mutant proteins with full bioactivity could improve the therapeutic efficacy[1,2], my new lysine-free EGF mutants are expected to improve the cytotoxic activity of cancer cells upon conjugation to NPs. Moreover, slight differences in EGFR-binding activities between the two mutants can be useful to investigate how binding characteristics as well as orientation control, result in cytotoxicity induction. Such information will be useful to elucidate the design rationale of more potent EGF-NP.

Gold nanoparticles (GNPs), a kind of novel metal nanoparticle ranging from one nanometer to several hundred nanometers, are extensively employed in various areas, including biology, medicine, and sensing, due to lower toxicity and good biocompatibility[3,4]. In addition, the GNPs with tunable properties (size and shape) and easy functionalization is the model platforms for biomedicine to investigate the interaction between cells and proteins[5]. Based on this, in this chapter, the GNPs were used to investigate the cytotoxic activity of the lysine-free EGF variants upon conjugating to NPs.

In order to conjugate the lysine-free EGF variants to the GNPs, the linker with the carboxyl group should be introduced to the GNPs. In addition, it was reported that the

GNPs were not stable in the physical condition and tended to agglomerate with enhanced toxicity to the cells[6]. Meanwhile, since the original charges of the GNPs are negative, positive-charged serum components in the culture media can be adsorbed to the surface of GNPs, altering the interaction between cells and GNPs conjugates[7,8]. Therefore, the stability of the GNPs conjugates is important. In this regard, the functionalization of GNPs with polyethylene glycol (PEG) is a promising strategy to boost their stability and inhibit the adsorption of the components in the culture medium[8–10]. In light of this, it is reasonable to functionalize the PEG to the surface of the GNPs. Apart from this, the density of the EGF conjugated to the GNPs would be another critical factor that can influence the outcome of cell response. For comparisons of the activity of the EGF-GNPs formed by EGF variants, the number of immobilized molecules must be the same, and it should also be characterized.

Considering these topics, in this chapter, I first functionalized the GNPs with PEG and PEG-COOH, then conjugated the EGF to GNPs by amide coupling. The dynamic light scattering and UV-Vis absorbance spectra were used to verify the functionalization of GNPs and the stability of EGF-GNPs. In addition, the surface charges of GNPs before and after EGF conjugation were also characterized. The number of EGF molecules was confirmed by the Micro-BCA assay. After that, I investigated the activities of the various EGF-GNPs, in terms of the phosphorylated extracellular signal-regulated kinase (ERK), binding ability, and cytotoxicity induction to verify whether the designed lysine-free EGF variants were effective and how the mutants influenced the activities of EGF-GNPs.

3.3 Materials and Methods

3.3.1 PEGylation of GNPs and chemical modification with

EGF

The procedure for producing the poly(ethylene glycol)-contained disulfide molecule (PEG-DSU) is described in the earlier article[11]. Briefly, two hundred fifty μL of 2.5 mM triethylamine (Wako, Osaka, Japan) was combined with 500 μL of 2.5 mM ω -methoxy-poly(ethylene glycol) amine (mPEG-NH₂, $M_w=5000$, NOF Corporation, Tokyo, Japan) and 250 μL of 1.25 mM dithiobis(succinimidyl undecanoate) (DSU, Dojindo, Kumamoto, Japan). The mixed solution was then subjected to an overnight reaction at room temperature using a rotating mixer at 8 rpm. Following, six mL of 15 nm GNPs (BBI Solution, Krumlin, UK) was centrifuged for 30 min at 10000 rpm to obtain a 60 μL solution. The centrifuged GNPs were subsequently functionalized using a rotating mixer operating at 8 rpm in a dimethyl sulfoxide (DMSO, Wako, Osaka, Japan) solution containing 2 mM poly(ethylene glycol) 2-mercaptoethyl ether acetic acid (SH-PEG-COOH, PEG average $M_n=5,000$ ($n\sim 110$), Sigma-Aldrich, MO, USA), and 2 mM PEG-DSU. Following an overnight reaction, the mixture was centrifuged to remove excess reagent and to obtain functionalized GNPs, which were subsequently washed three times with Milli-Q water for 30 minutes at 12000 rpm and dispersed in 600 μL 2-(*N*-morpholino) ethane sulfonic acid (MES, Dojindo, Kumamoto, Japan) buffer (pH = 5). After that, the mixture was supplemented with 150 μL of 0.2 M 1-ethyl-3-(3-dimethylaminopropyl) carbodiimide (EDC, Sigma-Aldrich) and 150 μL of 0.2 M *N*-hydroxy succinimide (NHS, Thermo Fisher Scientific, Waltham, MA, USA) and rocked at room temperature for 20 min. The activated GNPs were then added to phosphate-buffered saline (PBS) with 2 μM EGF after being centrifuged for three times with PBS at 12000 rpm for 30 min. At room temperature, the mixture was rocked for 2 h. The mixture was then centrifuged three times for 30 min each at a speed of 12000 rpm, followed by dispersing it in the 50 mM Tris (pH=7.6) to quench the remaining activated groups of the functionalized GNPs. Finally, after centrifugation, the concentrated EGF-GNPs were resuspended in the PBS for further

use. The formula used to calculate the amount of EGF on a single GNP is as follows:
number of EGF per GNP = (initially added EGF – remaining EGF in the supernatant)
/ total GNPs concentration. Given this, the UV-Vis spectrophotometer was used to measure the concentration of GNPs, and the Micro-BCA assay (Micro BCA™ Protein Assay Kit, Thermo Fisher Scientific) was used to determine the quantity of EGF in the supernatant following the instruction supplied by the manufacturer with a reference of commercial EGF (Sigma-Aldrich).

3.3.2 Characterization of GNPs and EGF-GNPs

The UV-Vis spectrophotometer was used to get the UV-Vis spectra (UV-2600, Shimadzu, Kyoto, Japan) of initial GNPs (no functionalization), PEGylated GNPs, and EGF-GNPs (WT-GNPs, RS-GNPs as well as SR-GNPs) either in PBS and culture medium. At the same time, the size distribution of these kinds of GNPs, which were obtained at different steps during functionalization and suspended in PBS and culture medium, were assessed by using dynamic light scattering (DLS, DLS-8000HAL, Otsuka Electronics, Osaka, Japan) under a 488 nm laser at a scattering angle of 90°. In addition, the surface charges of these GNPs in the PBS were also evaluated using the zeta potential analyzer (ELSZ-2000ZS, Otsuka Electronics Co., Ltd., Osaka, Japan).

3.3.3 Cell culture

The model cell employed in this system was the EGFR overexpressed cancer cell line A431 derived from epidermoid carcinoma (RCB022), which was bought from the RIKEN cell bank (Ibaraki, Japan). Then, A431 cells were then grown in 1% penicillin-streptomycin (Wako, Osaka, Japan) and 10% FBS (BioWest, Nuaille, France) in the Dulbecco's Modified Eagle's Medium (DMEM, Sigma-Aldrich) at 37°C in a humid environment with 5% CO₂.

3.3.4 ERK activity measurement using cell ELISA

A431 cells, with a density of 20000 per well, were grown in a 96-well plate at 37°C. After overnight incubation, the culture medium in the wells was replaced by 50 μ L fresh medium without FBS to serum-starve the A431 cells for 4 h. After that, the cells were treated with different samples (MEM and EGF-GNPs with different concentrations) for 5 min. Then, the solution in the well was extracted, followed by washing with PBS before being exposed to 150 μ L of 4% paraformaldehyde (PFA, Nacalai Tesque, Kyoto, Japan) solution at room temperature. After treatment for 20 minutes, 150 μ L of 0.5% Triton X-100 (Sigma-Aldrich, MO, USA) was added to permeabilize the cells for 20 min. After washing with PBS three times, 200 μ L of 2% BSA was added to the well for 1 h at room temperature. Afterward, the primary antibodies (Phospho-p44/42 MAPK (Erk1/2) (Thr202/Tyr204) rabbit mAb, 1:1000, Cell Signaling Technology, MA, USA) were then added to each well at a volume of 50 μ L for 2 h. After another round of washing, 100 μ L of anti-rabbit IgG alkaline phosphatase (Sigma-Aldrich, 1:3000) was added (1:3000). Subsequently, a further round of washing was followed by adding 100 μ L of anti-rabbit IgG alkaline phosphatase (Sigma-Aldrich, 1:3000). Subsequently, as a substrate, the 4-nitrophenylphosphate disodium hexahydrate (Sigma-Aldrich) was added with a volume of 100 μ L following a second round of washing. With the use of a microplate reader (Model 680, Bio-Rad, CA, USA), the signal was detected at 405 nm.

3.3.5 Binding Assay of EGF-GNPs

The surface plasmon resonance (SPR) instrument of Biacore X100 (GE Healthcare, Uppsala, Sweden) was used to perform the binding analysis of various GNPs (PEGylated GNPs, WT-GNPs, RS-GNPs, and SR-GNPs) at a concentration of 6 nM in degassed HBS-EP buffer (GE Healthcare). In this measurement, the CM5 sensor (GE Healthcare), which immobilized EGFR (Sigma-Aldrich) around 2000 RU, was

employed. The EGF-GNPs solution was injected for 2 min and allowed it flow over the surface of the EGFR-conjugated sensor chip at a rate of 30 $\mu\text{L}/\text{min}$ before being dissociated for 2 min via HBS-EP buffer. Subsequently, 5 mM sodium hydroxide and HBS-EP buffer were used for regeneration of the sensor chip with injection for 12 s and 30 s, respectively.

Finally, the BIAEvaluation software (GE Healthcare) was utilized to analyze the obtained sensorgrams, which monitored the changed binding response of the samples. The binding activities of various EGF-GNPs were compared 20 s after stopping the injection of EGF-GNPs.

3.3.6 Evaluation of cell viability

The viability of A431 cells was evaluated by using a cell proliferation assay kit (CellTiter 96[®]Aqueous Non-radioactive Cell Proliferation, Promega, WI, USA). Briefly, A431 cells with a density of 4000 cells/well were grown in a 96-well plate overnight. Subsequently, the culture medium was removed, followed by adding samples of soluble EGF, EGF-GNPs, and DMEM for 72 h. After gently removing the sample solution, the cells were washed twice with PBS twice. Finally, 100 μL of medium and 20 μL of a mixed solution, which was produced in accordance with the instructions of the manufacturer, were added to cells and allowed to culture with cells for 2 h. The signal was measured at 490 nm by using the above-mentioned microplate reader.

3.3.7 Statistical analysis of the data

A two-tailed *F*-test was employed to verify the variances of the results under the equal variance null hypothesis. To determine if the data for each group were statistically significant, a two-tailed student *t*-test was then employed. The *P*-value, which is lower than 0.05, was regarded as statistically significant.

3.4 Results

3.4.1 Conjugation of EGF with GNPs: preparation and characterization

Herein, the GNP was functionalized with two different polyethylene glycol (PEG) molecules (Figure 3-1), PEG-DSU and HS-PEG-COOH, with both molecular weights of around 5000. The PEG brushes, which were introduced by PEG-DSU, were used to prevent non-specific protein adsorption and enhance the stability of the GNPs when they were exposed to the culture medium. Meanwhile, the HS-PEG-COOH was utilized to conjugate the EGF molecule to the GNP by using amide coupling. Due to the presence of the DSU moiety, the COOH group was located somehow lower than the PEG brushes of PEG-DSU. However, I thought it was not a big problem for coupling the EGF molecule since the EGF molecule had been successfully conjugated to a much shorter DSU molecule (NHS-terminated disulfide) within the same molecular weight PEG-DSU brushes in the previous work from our group[12]. Moreover, it was also beneficial not to conjugate EGF to the outermost end of GNPs to prevent nanoparticle aggregation via the conjugated EGF molecule. Figure 3-1 depicts the process for conjugation of the EGF to the GNPs. First, GNPs (15 nm) were chemically modified using PEG-DSU and HS-PEG-COOH. Subsequently, the carboxyl groups of functionalized GNPs were activated by EDC/NHS, followed by reacting with EGF molecules to obtain EGF-GNPs conjugates.

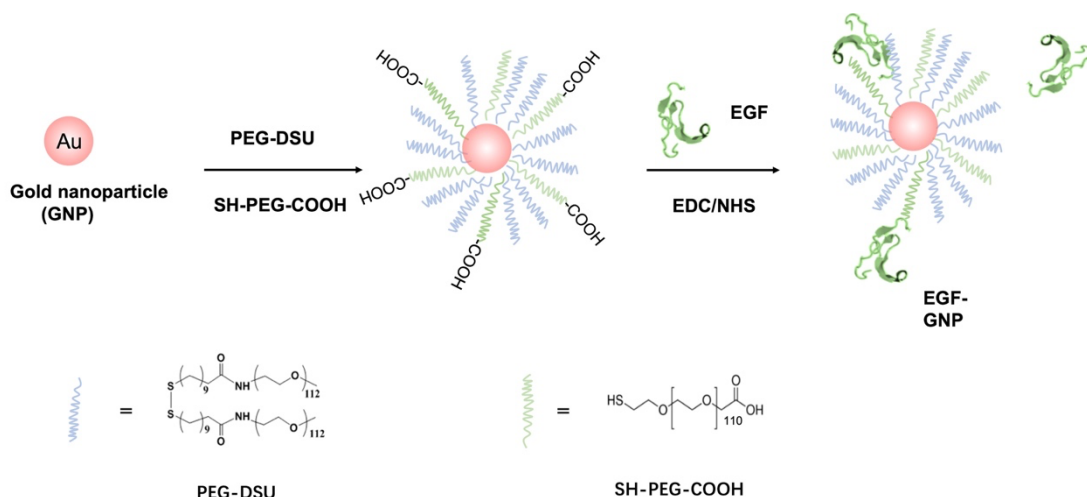


Figure 3-1 Schematic diagram of the procedure for preparation of EGF-GNPs conjugates. The EGF molecules conjugated to the GNPs by amide coupling. Adapted from Ref. [13], <https://doi.org/10.1080/14686996.2021.1944783>, under the terms of the CC BY license.

Subsequently, the number of conjugated EGF molecules in a single GNP was evaluated, and the result was illustrated in Figure 3-2. As shown, there was no significant difference between the three kinds of EGF (WT, SR, and SR), with a constant conjugated number of ~ 8 for the WT and EGF mutants. Meanwhile, the functionalization and stability of various GNPs (PEG-GNPs (PEGylated GNPs), EGF-GNPs, and non-functionalized GNPs) were characterized by using DLS (Table 3-1) and UV-Vis spectroscopy (Figure 3-3). The effective functionalization of GNPs was demonstrated by the increased diameter of EGF-GNPs and PEG-GNPs compared to the initial GNPs (non-functionalized GNPs) (Table 3-1, before). In addition, the polydispersity index (PDI), displayed in Table 3-1, was rather small (around 0.2), indicating the excellent homogenous distribution of the size of EGF-GNPs, which was considered acceptable in material and rather suitable to be applied in the drug delivery system[14]. Due to the electronic and optical properties of GNPs, an absorption peak near 520 nm can be observed when they were suspended in a solution that could be utilized to monitor the stability of the GNPs[15]. Based on this, I investigated the stability of prepared EGF-GNPs in the culture medium, considering that the serum in it would promote the aggregation of the GNPs. In this case, the stabilities of EGF-GNPs and PEG-GNPs, dispersed in the culture medium and PBS, were measured and

compared using UV-Vis spectroscopy. The obtained spectra of various GNPs in the different conditions of EGF-GNPs are displayed in Figure 3-3. From that, the spectra of EGF-GNPs, which were suspended in the culture medium, almost overlapped with that in the 0.1X PBS, confirming the high stability of the prepared EGF-GNPs. In addition, the unchanged diameter of EGF-GNPs in the culture medium compared with that in the PBS also verified the excellent stability of the EGF-GNPs (Table 3-1).

Meanwhile, the charges of the mutant EGF-GNPs were also verified and compared with that of WT-GNPs (Table 3-2). The zeta potential of the WT-GNPs and mutant EGF-GNPs (SR-GNPs and RS-GNPs) showed similar values; especially, there was no statistical difference between SR-GNPs and RS-GNPs. These results indicated that EGF-GNPs were successfully prepared, and they were stable under culture conditions with the almost same charges among various EGF-GNPs.

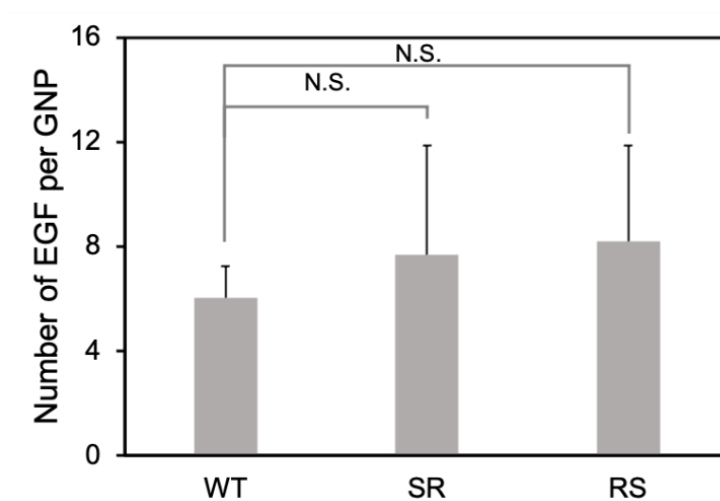


Figure 3-2 The quantified number of WT and EGF mutants immobilized to the nanoparticle. Based on the concentration of GNP and the reduction of the concentration of the EGF variants before and after conjugation, the number of immobilized EGF was estimated. The data reflect the mean and standard deviation of two triplicate experiments. The student's *t*-test determines the significance of the difference between the two groups. Reproduced from Ref. [13], <https://doi.org/10.1080/14686996.2021.1944783>, under the terms of the CC BY license.

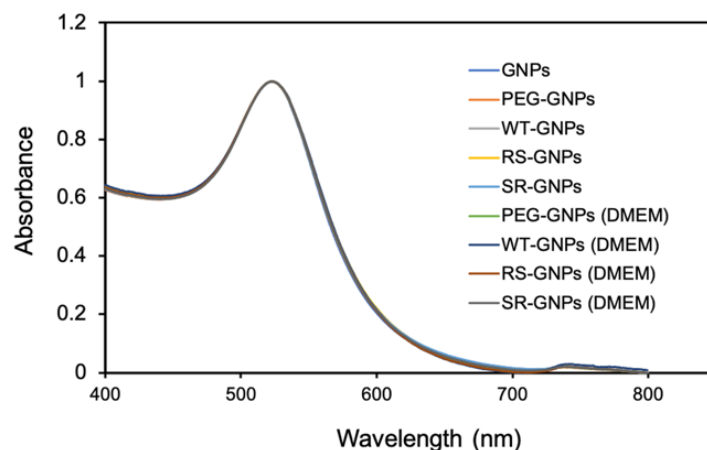


Figure 3-3 UV-Vis spectrum of EGF-GNPs and PEG-GNPs. The PEG-GNPs (no EGF conjugation) and various EGF-GNPs (WT-GNPs, RS-GNPs, and SR-GNPs) were dispersed in PBS and culture medium with serum, then measured by UV-Vis. DMEM in the Figure means the GNPs were dispersed in the medium. Reproduced from Ref. [13], <https://doi.org/10.1080/14686996.2021.1944783>, under the terms of the CC BY license.

Table 3-1 The polydispersity index (PDI) and hydrodynamic diameter of nanoparticles.

	Before		After	
	Size (nm)	PDI	Size (nm)	PDI
GNPs [†]	12.5 ± 2.2	0.06	---	---
PEG-GNPs [†]	25.4 ± 5.2	0.07	24.3 ± 5.2	0.14
WT-GNPs	29.1 ± 6.1	0.17	28.9 ± 5.9	0.20
SR-GNPs	28.0 ± 5.8	0.19	28.1 ± 5.7	0.19
RS-GNPs	28.1 ± 5.5	0.18	28.2 ± 5.7	0.21

*Number distribution was used to determine the average size of the nanoparticles by DLS measurements.

**Before represents the nanoparticles dispersed in the PBS, except the GNPs, which were dispersed in water. After represents the nanoparticles dispersed in the culture medium.

*** The data reflects the mean and standard deviation obtained from one experiment. Adapted from Ref. [13], <https://doi.org/10.1080/14686996.2021.1944783>, under the terms of the CC BY license.

Table 3-2 The zeta potential of functionalized GNP.

	PEG-GNPs	WT-GNPs	SR-GNPs	RS-GNPs
Zeta potential (mV)	-3.6 ± 0.8	-3.8 ± 0.5	-5.8 ± 1.0	-5.0 ± 1.0

[†] The PEG-GNPs and EGF-GNPs were dispersed in the PBS with a pH of 7.4.

[†] The data reflects the mean and standard deviation of triplicates of one sample. The *P* value between SR-GNPs and RS-GNPs was higher than 0.05.

3.4.2 Verification of bioactivity of EGF-GNPs

Similar to soluble EGF, I conducted an ELISA assay for the phosphorylated ERK level to evaluate the bioactivity of the prepared EGF-GNPs[16]. The relative amounts of ERK phosphorylation in A431 cells in response to different kinds of EGF-GNPs at various doses are shown in Figure 3-4A. The levels of phosphorylated ERK in A431 of all EGF-GNPs (WT-GNPs, RS-GNPs, and SR-GNPs) showed a concentration-dependent increase and revealed a saturation concentration at 6 nM. On the contrary, GNPs without EGF did not show such an increase for all the applied concentrations. Moreover, SR-GNPs exhibited noticeably greater ERK phosphorylation levels than WT-GNPs across the board concentration range of EGF-GNPs. However, the RS-GNPs showed slightly higher levels of phosphorylation than WT-GNPs at lower concentrations of nanoparticles (0.75 nM and 0.38 nM) (Figure 3-4B). These results showed that WT-GNPs, as well as SR-GNPs and RS-GNPs, preserved their bioactivity even after their conjugation to GNPs, but the mutant lysine-free EGF-GNPs exhibited somehow higher bioactivity against the cells.

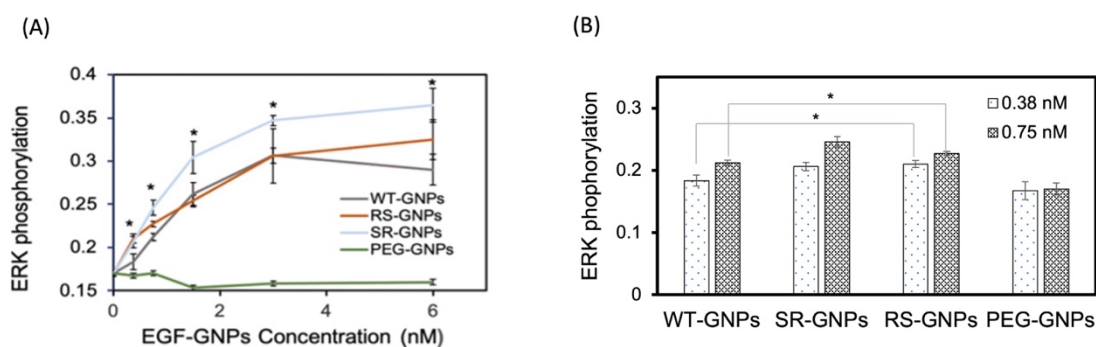


Figure 3-4 Verification of the bioactivities of different kinds of EGF-GNPs. The cell ELISA was used to evaluate the phosphorylated ERK level of the cells after treatment with different kinds of EGF-GNPs and PEG-GNPs for 5 min. (A) The phosphorylated ERK level at different concentrations of EGF-GNPs. (B) Bar graph of phosphorylated ERK levels of nanoparticles at 0.38 nM and 0.75 nM derived from A. The student's *t*-test determines the significance of the difference between the two groups ($*P < 0.05$). In A, the * represents of the significance of the difference between WT-GNPs and SR-GNPs. Mean \pm SD was obtained from three independent experiments. Adapted from Ref. [13], <https://doi.org/10.1080/14686996.2021.1944783>, under the terms of the CC BY license.

3.4.3 Binding analysis of EGF-GNPs

I then evaluated the binding activity of EGF-GNPs to EGFR by employing the SPR. Figure 3-5A demonstrates sensorgrams of samples. They represented the changes in binding response during the processes in that EGF-GNPs were associated with the EGFR (association phase) and dissociated from the EGFR (dissociation phase). The corresponding curve of the GNPs (control) without EGF conjugation completely overlapped with that of the buffer as a control, indicating that the GNPs themselves did not interact with the EGFR on the sensor chip. As opposed to that, the elevated binding responses in the sensorgrams can be observed for all the EGF-GNPs (WT-GNPs, RS-GNPs, and SR-GNPs) compared with the curves of background as well as GNPs, confirming the EGF can specifically interact with the EGFR even after conjugated to GNPs. It is worth noting that there is a little drop in the sensorgrams of the EGF-GNPs during the dissociation phase; this meant some of the captured EGF-GNPs kept interacting with EGFR even after switching the flow to the buffer solution. This was a

significant difference between EGF-GNPs and soluble EGF (without immobilization to GNPs); soluble EGF demonstrated the rapidly decreasing of the baseline with fast dissociation from the EGFR (Figure 2-7). This phenomenon might be due to the multivalent conjugation of the EGF to the GNPs, which dramatically enhanced the strength of the interaction between EGFR and EGF-GNPs, resulting in slowed dissociation. Given the small amount of the EGF-GNPs detected in the dissociation phase, it was difficult to determine the binding affinity of the EGF-GNPs in the standard method, like what I did for soluble EGF. Instead, I evaluated the binding activities of different kinds of EGF-GNPs at 20 s following the end of the injection of the EGF-GNPs solution to avoid the possible effect of the EGF-GNP existed in the buffer bulk. Figure 3-5B displays the quantified binding response of each sample. Compared to WT-GNPs, SR-GNPs, and RS-GNPs showed much stronger binding responses. Of note, the binding response of RS-GNPs was higher than that of the SR-GNPs. Given this, the binding activities of various EGF-GNPs were verified and compared. The results demonstrated that the lysine-free EGF mutant conjugated GNPs were more favorable to interact with EGFR than random-oriented conjugates based on wild-type EGF. Moreover, the two kinds of mutant EGF-conjugated GNPs showed different binding activity.

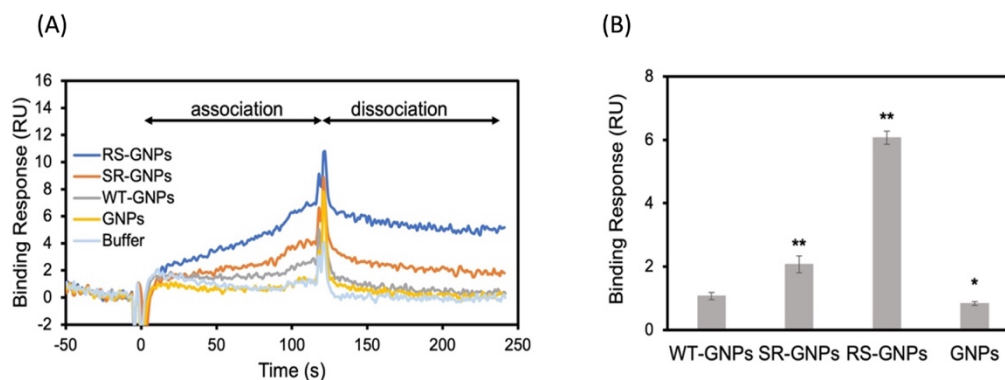


Figure 3-5 Binding analysis of GNPs (without EGF) and EGF-GNPs. (A) The monitored binding response of EGF-GNPs by using SPR. The sensorgrams were obtained by applying the different kinds of EGF-GNPs and GNPs at 6 nM to flow over the sensor chip with 120 s association followed by 120 s dissociation. As the reference, the buffer (HBS-EP) also flowed over the surface of the sensor chip. (B) Comparison of the binding activities of GNPs and different kinds of EGF-GNPs. The binding activities were determined by the binding response in the sensorgrams at 20 s after the end of the injection of the samples. The data reflects the mean and standard deviation of triplicates. The significance of the difference from WT-GNPs is determined by the student's *t*-test, which is indicated by the notations * ($P < 0.05$) and ** ($P < 0.01$). Reproduced from Ref. [17] with permission from Springer Nature, Copyright [2023].

3.4.4 Effects of growth inhibition of EGF-GNPs on A431 cells

A431 cells were exposed to various doses of different kinds of EGF-GNPs, PEG-GNPs (with no EGF), soluble EGF, and culture medium (MEM) to evaluate the impact on cell growth. The results, which are displayed in Figure 3-6A, depict the growth effects of the PEG-GNPs and EGF-GNPs at 6 nM against A431 cells. To compare the effects of EGF-GNPs on cell viability with soluble EGF, the concentration of soluble EGF concentration was set at 48 nM. With that, the effective EGF concentration for EGF and EGF-GNP become equivalent since all the EGF-GNP bear 8 EGF molecules per particle ($48 \text{ nM} = 6 \text{ nM} \times 8 \text{ molecule/GNP}$). As shown from it (Figure 3-6A), there was no significant difference in the viability between the cells treated with PEG-GNPs and untreated cells (the group labeled as “DMEM” in Figure 3-6).

On the contrary, cells treated with soluble EGF and EGF-GNP showed reduced viability compared to untreated cells and those treated with PEG-GNP. In light of the

results, it can be said that, in the chosen experimental settings (6 nM), GNPs alone had negligible influence on the viability of A431 cells. In contrast, the EGF immobilized on the GNPs could induce growth inhibition for the cells. EGF-GNPs treated cells, on the other hand, had lower viability than soluble EGF-treated cells, suggesting that EGF-GNPs had a greater growth inhibitory impact on cells than free EGF, which was consistent with earlier research[15]. Moreover, no statistically significant differences in the cell viability between WT-GNPs and mutant EGF-GNPs (RS-GNPs and SR-GNPs) were detected. However, it is worth noting that the cell viability for SR-GNPs was slightly lower than the others, indicating the SR-GNPs might have an enhanced growth inhibition effect than the WT-GNPs. Given this, an increased concentration (12 nM) of EGF-GNPs was applied to A431 cells, and the viability of the cells after treatment with EGF-GNPs was verified (Figure 3-6B). From it, cell viability generally exhibited a slight decline with the application of GNPs at this condition. In comparison to cells treated with WT-GNPs, SR-GNP treatment considerably increased cytotoxicity.

Furthermore, there was no discernible difference in the viability of cells treated with RS-GNPs and WT-GNPs. However, RS-GNPs induced a slight decrease in cell viability than WT-GNPs. These results showed that two lysine-free EGF-GNPs (SR-GNPs and RS-GNPs) had different effects on cell growth, whereas one lysine-free EGF conjugated GNPs (SR-GNPs) showed more potent growth inhibition in A431 cells than randomly oriented EGF conjugates (WT-GNPs), and the other one did not.

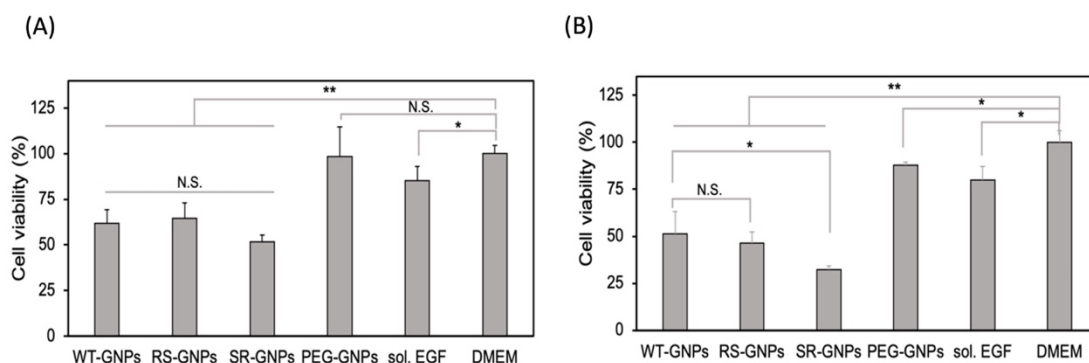


Figure 3-6 Cell viability measurement after treatment with EGF-GNP conjugates. To evaluate the viability of A431 cells, different samples, culture medium only (labeled as “DMEM”), soluble EGF (labeled as “sol. EGF”), PEG-GNPs (without EGF conjugation), and different kinds of EGF-GNPs were added and incubated with A431 cells for 3 days. The concentrations of 6 nM (A) and 12 nM (B) of EGF-GNPs and PEG-GNPs are shown. To keep the effective EGF concentration the same as EGF-GNPs, the soluble EGF concentration was adjusted at 48 nM and 96 nM, respectively. Each data point reflects the mean and standard deviation from three independent experiments (* $P < 0.05$, ** $P < 0.01$). Reproduced from Ref. [13], <https://doi.org/10.1080/14686996.2021.1944783>, under the terms of the CC BY license.

3.5 Discussion

Considering the possible random orientation of the EGF presented on the GNPs, it is attractive to produce site-specifically conjugated EGF conjugates to further improve their activity. The lysine-free EGF mutant with retained activity or even increased activity is promising to achieve this purpose.

Herein, I used wild-type EGF (WT) and previously designed lysine-free-EGF (SR and RS) to produce random conjugated WT-GNPs and site-specifically conjugated EGF-GNPs. Their effect on the activities of these EGF-GNPs were evaluated. After a series of characterization of nanoparticles, the results confirmed the high stability of the prepared EGF-GNPs in the culture condition. This means the length of the PEG (around 5000) is suitable for functionalizing GNPs since the PEG length is critical to determine the stability of the nanoparticles. Moreover, the high stability of the prepared EGF-GNPs was also important for following cellular studies since particle aggregation could interfere with the interaction of EGF-GNP with cells. On the other

hand, EGF-GNPs displayed almost the same value of zeta potential among WT-GNPs (-3.8 ± 0.5 mV), SR-GNPs (-5.8 ± 1.0 mV), and RS-GNPs (-5.0 ± 1.0 mV) (Figure 3-2). The slightly lower zeta potential value for WT-GNPs than the other two may be due to the replacement of endogenous lysine residues with serine or arginine in the mutant-GNPs. This substitution changes the two charged lysine residues to one charged arginine and one neutral serine; thereby, the net positive charge decreases for the mutants in physiological pH. However, due to the slight difference in the zeta potential, I considered its influence on the interaction of EGF-GNPs and cells was minimum. Especially between SR-GNPs and RS-GNPs, there was no statistical difference in zeta potential. Also, the number of conjugated EGF on a gold nanoparticle was constant for all EGF variants. It is essential to ensure the immobilized EGF number on the GNPs among EGF variants since the ligand density of conjugates is considered another important factor that could influence cell/conjugates interaction[18].

Under these conditions, the binding activities (Figure 3-5) and bioactivities of different EGF-GNPs (Figure 3-4) were analyzed. Based on the binding response, the EGF-GNPs were ordered in the following: RS-GNPs > SR-GNPs > WT-GNPs, whereas the rank of the binding affinity of the soluble EGF was the following: RS > SR > WT (Table 2-2). Since these binding assays were conducted in vitro with the extracellular domain of the EGFR, it was considered that no other factor influenced the EGF-EGFR interaction. The different trend of the binding activities between EGF and their conjugates indicates that the intrinsic binding properties of the EGF mutants could also affect the binding activity of the EGF-GNPs. On the other hand, since the WT and SR in the soluble form have a comparable activity of the binding, the elevated binding activity of SR-GNPs, compared with WT-GNPs, indicated the successful control of the orientation of EGF on the GNPs by using lysine-free EGF. Moreover, this strategy can improve the binding activity of the EGF-GNPs compared to the randomly oriented EGF-GNPs. Meanwhile, the RS-GNPs displayed more excellent binding responses than WT-GNPs and SR-GNPs, probably due to the increased binding affinity of soluble

RS compared to WT and SR. Therefore, I can say the development of new lysine-free mutants alter (even enhance) the intrinsic binding characteristics probably ascribing to its favorable orientation. Of note, the binding response obtained from the EGF-GNPs (Figure 3-5) was much lower than soluble EGF (Figure 2-7); it might be due to the restricted penetration of the EGF-GNPs into the dextran matrix of the sensor chip (CM5) than the smaller size soluble EGF. This resulted in inefficient interaction of EGF-GNP with EGFR[19]. At the same time, the reduced signal of GNP binding was a good indication that the modification of PEG on the surface of GNP could significantly inhibit nonspecific adsorption to the substrate, as reported previously[8–10]. The bioactivities of the different EGF-GNP conjugates were then assessed with regard to ERK phosphorylation. The obtained ranking of their bioactivities was ordered as follows: SR-GNPs > RS-GNPs \cong WT-GNPs (Figure 3-4). These results indicate that the lysine-EGF conjugates can improve the capacity of the EGF-GNPs to activate EGFR signaling. This trend, however, did not coincide with the trend of binding activities of EGF-GNPs, which was mentioned above. Moreover, the capability of EGF-GNPs for induced growth inhibition of A431 displayed a different trend from that of the binding activity against EGFR (Figure 3-6). Of note, SR-GNPs showed enhanced cytotoxicity than WT-GNPs. These results in this chapter confirmed that lysine-free EGF mutants could be used to achieve orientation-controlled EGF-GNPs with improved binding activity, bioactivity, and cytotoxicity. At the same time, it also indicates that the increased binding activity with EGFR is not the sole determinant to enhance bioactivity and cancer cell cytotoxicity of EGF-GNPs. It clearly shows the synergistic effect of the mutant-derived activity alteration of the EGF molecule and the orientation. This prompted me to further study the possible mechanism for the cytotoxicity induction of various EGF-GNPs to clarify the important design rationale of this recombination strategy in this new anti-cancer modality.

3.6 Conclusion

In this work, I prepared the EGF conjugates by using lysine-free EGF mutants for orientation control to improve anti-cancer effects. After being applied in the A431 cells (EGFR-overexpressed skin cancer cell line), the one lysine-free EGF conjugates (SR-GNPs) revealed improved biological activity as well as growth inhibition, but RS-GNPs did not when compared with WT-GNPs (randomly oriented EGF conjugates). This means orientation control is not the sole answer for cytotoxicity enhancement, and the mutant-derived alteration of the intrinsic activity of EGF is another factor that should be considered. Since there is a different trend of binding activity and binding affinity between SR-GNPs and RS-GNPs, it may be an indication that something is happening. However, the improved cytotoxicity of SR-GNPs strongly validates the strategy of site-specific conjugation EGF on GNPs by using lysine-free EGF, which I proposed in the hypothesis. Moreover, the prepared SR-GNPs can be used as a potential therapeutic drug for cancer treatment.

Reference

- 1 Yamamoto, Y., Tsutsumi, Y., Yoshioka, Y., Nishibata, T., Kobayashi, K., Okamoto, T., Mukai, Y., Shimizu, T., Nakagawa, S., Nagata, S., et al. (2003) Site-specific pegylation of a lysine-deficient TNF- α with full bioactivity. *Nat. Biotechnol.* **21**, 546–552.
- 2 Narimatsu, S., Yoshioka, Y., Watanabe, H., Masano, T., Morishige, T., Yao, X., Tanabe, A., Tsunoda, S. ichi, Tsutsumi, Y., Mukai, Y., et al. (2011) Lysine-deficient lymphotoxin- α mutant for site-specific PEGylation. *Cytokine* **56**, 489–493.
- 3 Daraee, H., Eatemadi, A., Abbasi, E., Aval, S. F., Kouhi, M. and Akbarzadeh, A. (2016) Application of gold nanoparticles in biomedical and drug delivery. *Artif. Cells, Nanomedicine Biotechnol.* **44**, 410–422.
- 4 Bansal, S. A., Kumar, V., Karimi, J., Singh, A. P. and Kumar, S. (2020) Role of gold nanoparticles in advanced biomedical applications. *Nanoscale Adv.* **2**, 3764–3787.
- 5 Jazayeri, M. H., Amani, H., Pourfatollah, A. A., Pazoki-Toroudi, H. and Sedighimoghaddam, B. (2016) Various methods of gold nanoparticles (GNPs) conjugation to antibodies. *Sens. Bio-Sensing Res., The Authors* **9**, 17–22.
- 6 Alkilany, A. M. and Murphy, C. J. (2010) Toxicity and cellular uptake of gold nanoparticles: What we have learned so far? *J. Nanoparticle Res.* **12**, 2313–2333.
- 7 Lee, Y. K., Choi, E. J., Webster, T. J., Kim, S. H. and Khang, D. (2014) Effect of the protein corona on nanoparticles for modulating cytotoxicity and immunotoxicity. *Int. J. Nanomedicine* **10**, 97–113.
- 8 Patlolla, A. K., Kumari, S. A. and Tchounwou, P. B. (2019) A comparison of poly-ethylene-glycol-coated and uncoated gold nanoparticle-mediated hepatotoxicity and oxidative stress in sprague dawley rats. *Int. J. Nanomedicine* **14**, 639–647.

-
- 9 Niidome, T., Yamagata, M., Okamoto, Y., Akiyama, Y., Takahashi, H., Kawano, T., Katayama, Y. and Niidome, Y. (2006) PEG-modified gold nanorods with a stealth character for in vivo applications. *J. Control. Release* **114**, 343–347.
 - 10 Manson, J., Kumar, D., Meenan, B. J. and Dixon, D. (2011) Polyethylene glycol functionalized gold nanoparticles: The influence of capping density on stability in various media. *Gold Bull.* **44**, 99–105.
 - 11 Nakanishi, J., Nakayama, H., Shimizu, T., Ishida, H., Kikuchi, Y., Yamaguchi, K. and Horiike, Y. (2009) Light-regulated activation of cellular signaling by gold nanoparticles that capture and release amines. *J. Am. Chem. Soc.* **131**, 3822–3823.
 - 12 Yamamoto, S., Iwamaru, Y., Shimizu, Y., Ueda, Y., Sato, M., Yamaguchi, K. and Nakanishi, J. (2019) Epidermal growth factor-nanoparticle conjugates change the activity from anti-apoptotic to pro-apoptotic at membrane rafts. *Acta Biomater.* **88**, 383–391.
 - 13 Zhang, A. and Nakanishi, J. (2021) Improved anti-cancer effect of epidermal growth factor-gold nanoparticle conjugates by protein orientation through site-specific mutagenesis. *Sci. Technol. Adv. Mater.* **22**, 616–626.
 - 14 Danaei, M., Dehghankhold, M., Ataei, S., Hasanzadeh Davarani, F., Javanmard, R., Dokhani, A., Khorasani, S. and Mozafari, M. R. (2018) Impact of particle size and polydispersity index on the clinical applications of lipidic nanocarrier systems. *Pharmaceutics* **10**, 1–17.
 - 15 Wu, L., Yu, X., Feizpour, A. and Reinhard, B. M. (2014) Nanoconjugation: A materials approach to enhance epidermal growth factor induced apoptosis. *Biomater. Sci.* **2**, 156–166.
 - 16 Kim, W., Na, K.-Y., Lee, K.-H., Lee, H. W., Lee, J. K. and Kim, K.-T. (2017) Selective uptake of epidermal growth factor-conjugated gold nanoparticle (EGF-GNP) facilitates non-thermal plasma (NTP)-mediated cell death. *Sci. Rep.* **7**, 10971.

-
- 17 Zhang, A., Abdellatef, S. A. and Nakanishi, J. (2023) Mechanistic investigation into selective cytotoxic activities of gold nanoparticles functionalized with epidermal growth factor variants. *Anal. Sci.* **39**, 395–405.
- 18 Zhang, Q. and Reinhard, B. M. (2018) Ligand Density and Nanoparticle Clustering Cooperate in the Multivalent Amplification of Epidermal Growth Factor Receptor Activation. *ACS Nano* **12**, 10473–10485.
- 19 Tassa, C., Duffner, J. L., Lewis, T. A., Weissleder, R., Schreiber, S. L., Koehler, A. N. and Shaw, S. Y. (2010) Binding affinity and kinetic analysis of targeted small molecule-modified nanoparticles. *Bioconjug. Chem.* **21**, 14–19.

Chapter 4

Mechanistic study of cytotoxic induction by EGF-GNP

4.1 Summary

Lysine-free epidermal growth factor (EGF) mutants were assumed to facilitate the interactions between the EGF receptor (EGFR) and nanoparticle conjugates due to the defined conjugation at N-terminal. Given this, two mutants were designed and utilized to prepare the EGF-GNPs in the last two chapters. Surprisingly, I found that the anticancer activities of mutants heavily rely on their types and controlled orientation. As a result, one mutant showed the most profound anticancer activity. However, the underlying mechanism for selectively enhanced cytotoxicity in the EGF mutant still needs to be fully understood. This study systematically investigated the interactions of (wild-type EGF and EGF mutants)-conjugated GNPs with A431 cancer cells regarding EGFR activation, cellular uptake, and trafficking. The results revealed that the increased cytotoxic induction of mutant EGF-conjugates originated from their preferred stimulation of the clathrin-independent endocytosis, indicating that besides focusing on controlled orientation, further consideration also had to be given to the selectivity of endocytic pathway to improve the anticancer effects in this modality.

4.2 Introduction

Assuming that one of the major reasons for the low cytotoxic activities of the previous EGF-GNPs against tumor cells is uncontrolled orientation on the surface of

GNPs, in the last chapters, two kinds of lysine-free EGF mutants, SR and RS, were designed. As I hypothesized, the orientation control on the GNP surface was successful for both mutants, and the net binding affinities of the mutant EGF-GNPs became larger than randomly oriented WT-GNPs. Interestingly, however, the enhanced cytotoxicity over WT-GNPs was only observed for SR-GNPs, and not for RS-GNPs, even though soluble RS-EGF gained higher binding activity than WT and SR both in the soluble and GNP conjugate forms. Such inconsistency between binding activity and cytotoxicity in mutant EGF-GNPs indicates that the overall efficiency to exhibit a cytotoxic effect on tumor cells might not be simply determined by the binding ability of EGF-GNPs, with cell-surface EGFR, rather there exist other factors that is essential to alter the efficiency of EGF-GNPs in cytotoxic induction. This is a critical issue for the future application of EGF-GNPs as anti-cancer drugs.

To this end, in this chapter, I addressed the origin of different cytotoxic abilities between SR-GNPs and RS-GNPs in A431 cells, a model cell line overexpressing EGFR. Together with WT-GNPs, multiple analytical methodologies, including a phosphorylation array, western blotting, inductively coupled plasma mass spectrometry (ICP-MS), and immunofluorescence, were employed to analyze the EGFR activation, cellular uptake, and EGFR trafficking. The obtained results demonstrated that receptor trafficking played a vital role in the cytotoxic induction of EGF-GNPs, disclosing a distinctive characteristic compared to traditional EGFR inhibitors.

4.3 Materials and Methods

4.3.1 Materials and reagents

The three kinds of EGF variants (WT, SR, and RS) and their corresponding conjugates EGF-GNPs, were prepared according to the procedures mentioned in the previous chapters. For all EGF variants, the same number of the EGF molecule was

conjugated to the surface of GNPs.

4.3.2 Cell culture

The model cell employed in this system was the EGFR-overexpressing cancer cell line A431 (RCB022), which was bought from the RIKEN cell bank (Ibaraki, Japan). A431 cells were then grown in the Dulbecco's Modified Eagle's Medium (DMEM, Sigma-Aldrich, MO, USA) with 10% fetal bovine serum (FBS, BioWest, Nuaille, France) plus 1% penicillin-streptomycin (P/S, Wako, Osaka, Japan) in a humid environment with 5% CO₂ at 37°C.

4.3.3 EGFR phosphorylation assay

The EGFR phosphorylation array (human EGFR Phosphorylation Array C1, RayBiotech, Norcross, USA) was applied to evaluate the EGFR phosphorylation state of A431 cells after treatment with EGF-GNPs. Briefly, A431 cells were grown in a 10 cm plate until confluency reached about 80%, then starved for 4 h. Afterwards, 6 nM of EGF-GNPs and control PEG-functionalized GNPs were applied to the plate and the cells were incubated for 10 minutes. Then, the solution in the dish was discarded, followed by washing with ice-cold PBS. Afterward, the cells are lysed and applied to the membrane according to the protocol of the phosphorylation array provided by the manufacturer. Finally, a live imaging software version 3.2 on an IVIS imaging system (Xenogen IVIS® Lumina II, Summit Pharmaceuticals, Tokyo, Japan) was used to obtain the image.

Western blot was used to measure the phosphorylation levels at the Y845, Y1068 as well as Y1173 sites of EGFR. In brief, A431 cells with a density of 6×10^5 cells per well were seeded in a 6-well plate overnight, followed by starvation for 4 h. The different types of EGF-GNPs with a concentration of 6 nM were applied to the wells to react for 20 h followed by washing twice with ice-cold PBS. Afterward, the ice-cold

Radio Immuno Precipitation Assay (RIPA, Nacalai Tesque, Kyoto, Japan) buffer was added to scrape off the cells from the wells before being collected into a new sample tube followed by centrifugation at 4°C (16000 g, 10 min). Subsequently, the supernatant of the sample in the tube was transferred to a new tube. Then, the DC protein assay was used to measure the protein concentration of the supernatant, followed by loading to the sodium dodecyl sulfate (SDS) polyacrylamide gel (Mini-PROTEAN® TGX™ Precast Protein Gels, 10%, Bio-Rad, CA, USA). Then, electrophoresis was used to separate the protein before being transferred to a nitrocellulose membrane (Bio-Rad, CA, USA). Afterward, 5% bovine serum albumin (BSA, Wako, Osaka, Japan) was applied to the membrane to block the membrane. Thereafter, they were incubated at 4°C overnight with the primary antibodies against pY845 (anti-phospho Y845, Cell Signaling Technology (CST), MA, USA, 1:1000), pY1068 (anti-phospho Y1068, CST, 1:1000), pY1173 (anti-phospho Y1068, CST, 1:1000), and anti-GAPDH (Abcam, Cambridge, UK, 1:1000). Subsequently, the horseradish peroxidase (HRP)-conjugated secondary antibodies (Jackson ImmunoResearch Co., PA, USA) were applied to the membrane and allowed to incubate for 2 h. Then, 0.1% Tween-20 contained Tris-buffered saline was used to wash the membrane. Eventually, utilizing a chemiluminescence substrate (Super Signal™ West Dura Extended Duration Substrate, Thermo Fisher Scientific, IL, USA), the HRP signal of the membrane was detected by using an IVIS imaging system, which was mentioned before.

4.3.4 Cellular uptake measurements

Inductively coupled plasma mass spectrometry (ICP-MS, Agilent 7850, Agilent, CA, USA) was employed to analyze the cell uptake of different kinds of EGF-GNPs by A431 cells. Shortly, cells were seeded in a 24-well plate with a density of 2×10^5 cells/well. Following overnight incubation, GNPs functionalized with EGF variants, including WT (WT-GNPs), RS (SR-GNPs), and SR (RS-GNPs), or those without EGF

(PEG-functionalized GNP, labeled as “GNPs” in the Figure) were introduced to the wells with 6 nM nanoparticle concentration and allowed to incubate with cells for 24 h. Following removing the sample solution from the well, the cells underwent two times washing with PBS before being harvested with trypsin. After counting the cell number, the cells were pelleted by centrifugation. The supernatant in the tube was discarded, and the samples were dissolved overnight in 0.5 mL aqua regia before diluting them to 5 mL with Milli-Q water. Then, the gold content in the sample was measured using ICP-MS. Finally, the number of GNP in one cell was used to represent the content of gold. The formula below was used to determine how many uptaken GNPs are present in each cell: $\text{GNP per cell} = \text{total gold mass} / \text{average mass of a single GNP} / \text{number of cells}$.

4.3.5 Immunofluorescence staining

With a density of 4×10^4 cells/well, the A431 cells were added to an 8-well chamber slide and cultured at 37°C overnight. On the next day, the culture medium was replaced with the fresh medium without serum, followed by starvation of the cells for 4 h. After that, 6 nM of EGF-conjugated GNPs and control PEG-functionalized GNPs without EGF modification were reacted with cells for 3 h, followed by washing with PBS. Then, the 4% paraformaldehyde (PFA, Nacalai Tesque) was added to fix the cells at room temperature. After 20 min incubation, 0.5% Triton X-100 (Sigma-Aldrich, MO, USA) was utilized to permeate the cells for 10 min. After that, 2% BSA was employed to block the cells, followed by incubation with anti-clathrin (Abcam, Cambridge, UK, 1:200) and anti-EGFR (D38B1, CST, 1:200) at 4 °C for 24 h. After that, the cells were washed with buffer, followed by adding the Alexa Fluor 568-labeled goat anti-rabbit polyclonal IgG (H+L) (Invitrogen, CA, USA, 1:500), which specifically recognize anti-EGFR antibodies, and the Alexa Fluor 488-labeled chicken anti-mouse polyclonal IgG (H+L) (Invitrogen, 1:500), which specifically recognize anti-clathrin. After 1 h incubation, the cells were rewashed. After that, the nuclei of the cells were stained by

the Hoechst 33342 (Invitrogen, 1:4000) for 10 min. LSM 900 Airyscan confocal laser-scanning microscope (Carl Zeiss, Oberkochen, Germany) with a 63 \times oil immersion objective (numerical aperture = 1.4, Carl Zeiss) was used for imaging. Afterward, the images were processed via Zen Software (Blue edition @ Carl Zeiss microscope, 3.4.91). The Coloc 2 Plugin in Fiji (W. Rasband, National Institutes of Health, Bethesda, MD, USA) was used to analyze Pearson's R-value (colocalization index) by measuring the pixel-by-pixel covariance of signal in the images from 13–19 cells.

4.3.6 Data analysis

A two-tailed *F*-test under a equal variance null hypothesis was performed to determine the variances of the results. After that, a two-tailed student *t*-test was employed to ascertain if the results were statistically significant. A *P*-value < 0.05 (*) and a *P*-value < 0.01 (**) indicated statistical significance.

4.4 Results

4.4.1 Evaluation of EGFR phosphorylation of A431 cells

The EGFR undergoes phosphorylation at certain residues upon ligand binding, which is crucial for signal transduction to the downstream[1]. Hence, the phosphorylation patterns of the EGFR show how the receptor is activated. Given this, by employing A431 cells, I initially examined 16 probable sites of phosphorylation of the human EGFR family to evaluate and monitor the changes related to the EGFR activation after treatment of different kinds of EGF-GNPs (Figure 4-1). Figure 4.1A–C demonstrates similar patterns between WT-GNPs and mutant EGF conjugated-GNPs (RS-GNPs and SR-GNPs) in terms of EGFR phosphorylation. Especially, compared to control PEG-functionalized GNPs, the significant increase in the phosphorylation levels were detected for in EGFR at tyrosine 1173 (Y1173) and tyrosine 845 (Y845).

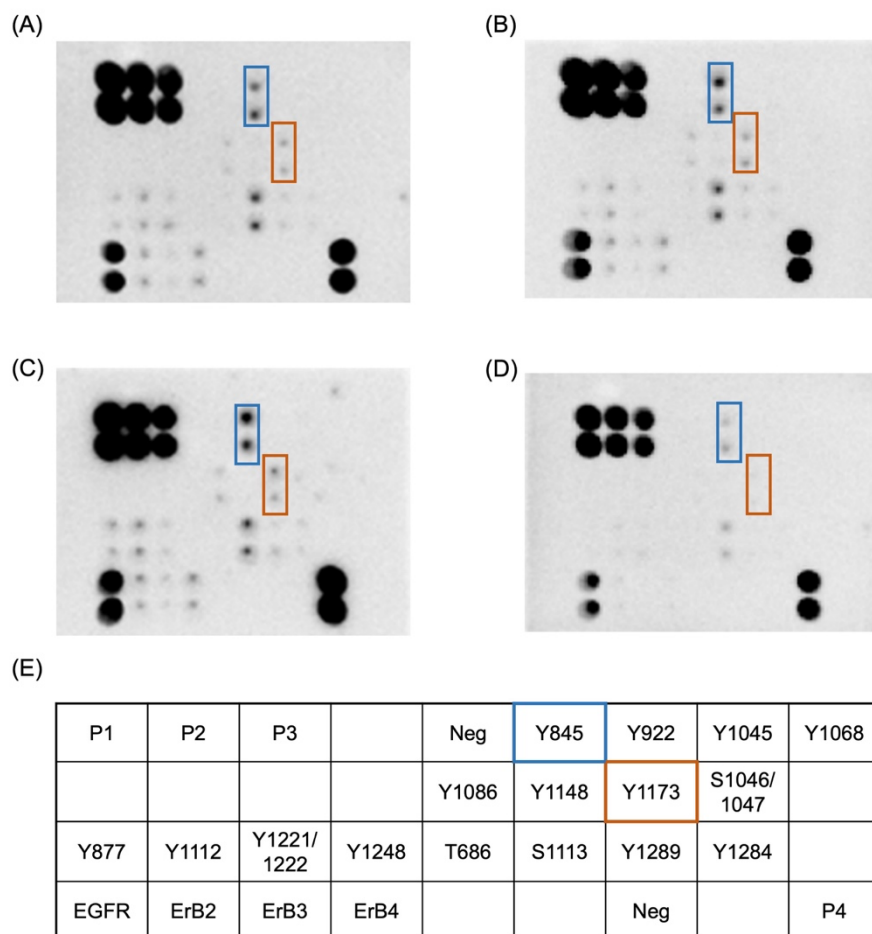


Figure 4-1 Monitoring the state of EGFR phosphorylation using the EGFR phosphorylation array. At a concentration of 6 nM of GNPs, the WT-GNPs (A), SR-GNPs (B), RS-GNPs (C) as well as PEG-functionalized GNPs (D) were applied to the A431 cells. The EGFR activation states were evaluated after 10 min treatment. (E) Human EGFR phosphorylation array map. P: positive spots. Neg: negative spot. EGFR: the amount of EGFR expression. Phosphorylation sites on the EGFR include Y845, Y992, Y1045, Y1068, Y1086, Y1148, Y1173, and S1046/1047. ErB2: the amount of ErB2 expression. ErB2 has the following phosphorylation sites: Y877, Y1112, Y1221/1222, Y1248, T686, and S1113. ErB3: the amount of ErB3 expression Y1289: ErB3 phosphorylation site. ErB4: the amount of ErB4 expression. Y1284: an ErB4 phosphorylation site. Reproduced from with Ref. [2] permission from Springer Nature, Copyright [2023].

I further quantitatively compared the phosphorylation of Y845 and Y 1173 among WT-GNPs, RS-GNPs, and SR-GNPs using western blotting. In addition, Y1068 residue serves as an essential autophosphorylation site of EGFR, which researchers often characterize to evaluate the state of EGFR activation[3]. Given this, the phosphorylation level at Y1068 was also quantified. According to Figure 4-2, the phosphorylated levels at Y845 in RS-GNPs treated cells and Y1173 in SR-GNPs treated

cells were more outstanding than in WT-GNPs. Meanwhile, compared with RS-GNPs and WT-GNPs, marginally weaker signaling of the EGFR phosphorylation at the Y1068 site in SR-GNPs was observed. Nevertheless, no significant differences could be observed between WT-GNPs, RS-GNPs, and SR-GNPs.

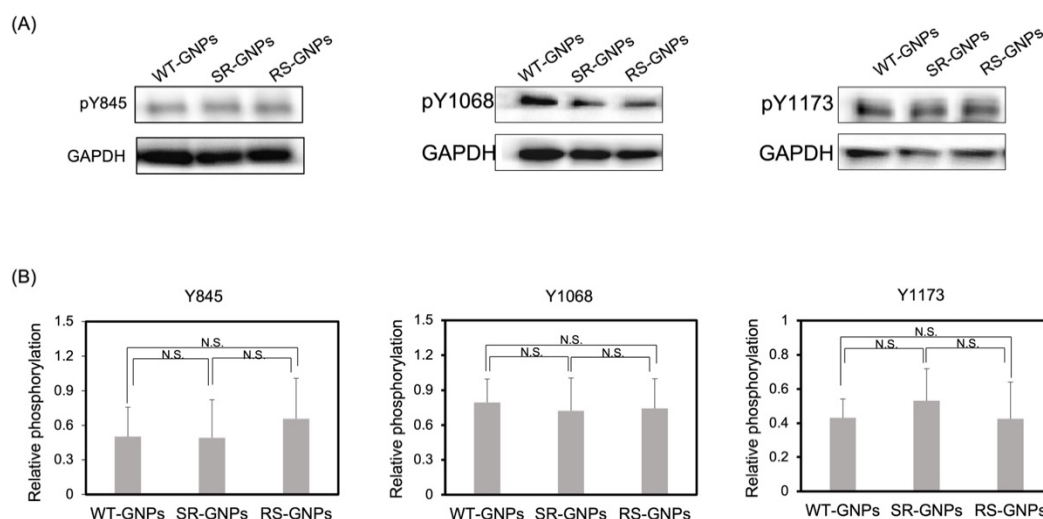


Figure 4-2 Quantification of EGFR phosphorylation. The A431 cells were treated with three different kinds of EGF-GNPs at a concentration of 6nM for 24 h. The representative images of western blot (A) and quantified levels of EGFR phosphorylation (B) at Y845, Y1068 as well as Y1173. The protein level of GAPDH was utilized to normalize the phosphorylation level of EGFR. Mean \pm SD was calculated from at least three independent experiments. Student's *t*-test was used to evaluate the statistical differences. Reproduced from with Ref. [2] permission from Springer Nature, Copyright [2023].

4.4.2 Cellular uptake of EGF-GNPs by A431 cells

The persistent EGFR activation by uptaken EGF-NPs in endosomes has been proposed as one of the mechanisms of EGF-NPs-induced apoptosis[4]. Accordingly, I looked at how WT-GNPs and mutant EGF-GNPs were taken up by A431 cells. ICP-MS was utilized to assess the cellular uptake of these different kinds of EGF-GNPs and the PEG-functionalized GNPs (without EGF). As seen in Figure 4-3, the GNPs after conjugation with EGF variants can be uptaken by A431 cells with a number of $\sim 10^4$ GNPs/cell, whereas the uptake of PEG-functionalized GNPs (without EGF) by A431 cells was noticeably lower (8×10^2 GNPs/cell) than them. This was an evidence

that the GNP with EGF modification exhibited increased uptake by the cells. Furthermore, when comparing the amount of uptaken EGF-GNPs among different EGF variants, WT-GNP had the lowest uptake, SR-GNP showed moderate, and RS-GNP showed the highest uptake in A431 cells. These results indicated that cellular uptake might also not be the reason for the enhanced cytotoxicity of the SR-GNPs.

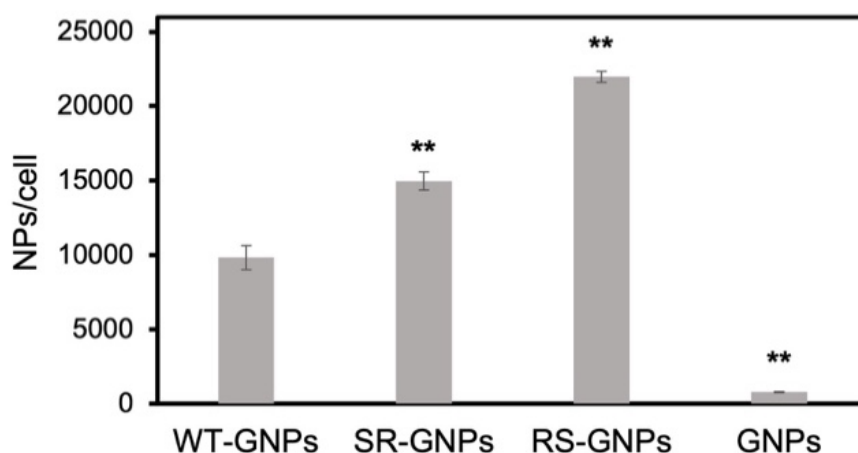


Figure 4-3 Quantification of the cellular uptake of EGF-GNPs and GNPs. A431 cells were treated with EGF variant (WT, SR, or RS)-conjugated GNPs and PEG-functionalized GNPs (labeled as “GNPs”) with a concentration of 6 nM for 24 h before being quantified by ICP-MS. Uptake value represented the number of GNPs in one cell (NPs/cell). Student’s *t*-test was used to evaluate the statistical difference from WT-GNPs. Mean \pm SD was derived from three independent experiments. **: $P < 0.01$. Reproduced from with Ref. [2] permission from Springer Nature, Copyright [2023].

4.4.3 EGFR and clathrin-coated vesicle colocalization analysis

There are two major endocytosis pathways: clathrin-independent mediated endocytosis and clathrin-mediated endocytosis for the EGF-GNPs to enter cells, demonstrated by early studies[4,5]. Using different types of cells with different EGFR overexpression is one possibility that contributes to the variance in the trafficking pathway. Moreover, by changing the electrostatic properties of the NPs[6] as well as the multivalency of the ligands on the NPs[7], endocytic routes can be also switched from one to another. Given this, I expected that EGF-GNPs with different binding

properties against EGFR, specifically WT-GNPs, SR-GNPs, and RS-GNPs, can also change the interaction between EGF-GNPs and cells, leading to the alteration of pathways of endocytic trafficking. In order to investigate this possibility, EGFR endocytic trafficking was examined after stimulating the cells with different EGF variants-conjugated GNPs. Clathrin-coated vesicles and EGFR were detected using immunofluorescent staining. The Pearson's correlation coefficient, also namely Pearson's R, ranges from -1 to 1 and can be used to determine how strong a linear correlation between two variables is[8,9]. Accordingly, Pearson's R-value measures the degree of colocalization between clathrin and EGFR after stimulating with PEG-functionalized GNPs (without EGF conjugation, labeled as "GNPs" in the Figure) or different kinds of EGF-GNPs (Figure 4-4). Of note, the colocalization index using Pearson's R is a relative value highly dependent on the sample condition that should be compared with the control. As a result of stimulation with RS-GNPs and WT-GNPs, the colocalization index significantly increased to 0.73 and 0.74, respectively, compared to the values stimulated with control sample, including medium or PEG-functionalized GNPs (0.6). Thereby, the RS-GNPs and WT-GNPs are expected to use the clathrin-dependent pathway based on the elevated colocalization index, which means a stronger correlation between clathrin and EGFR than the control samples. On the other hand, SR-GNPs maintained the colocalization index of 0.61, similar to the control. Considering the above ICP-MS results regarding minimum uptake of PEG-functionalized GNPs and significantly high uptake of SR-GNPs (Figure 4-3), the colocalization index of 0.6 for the PEG-functionalized GNPs represented the colocalization level at the resting state. In contrast, no increase in the colocalization index (0.61) for SR-GNPs indicated the SR-GNPs was more preferentially endocytosed through clathrin-independent pathway than WT-GNPs and RT-GNPs.

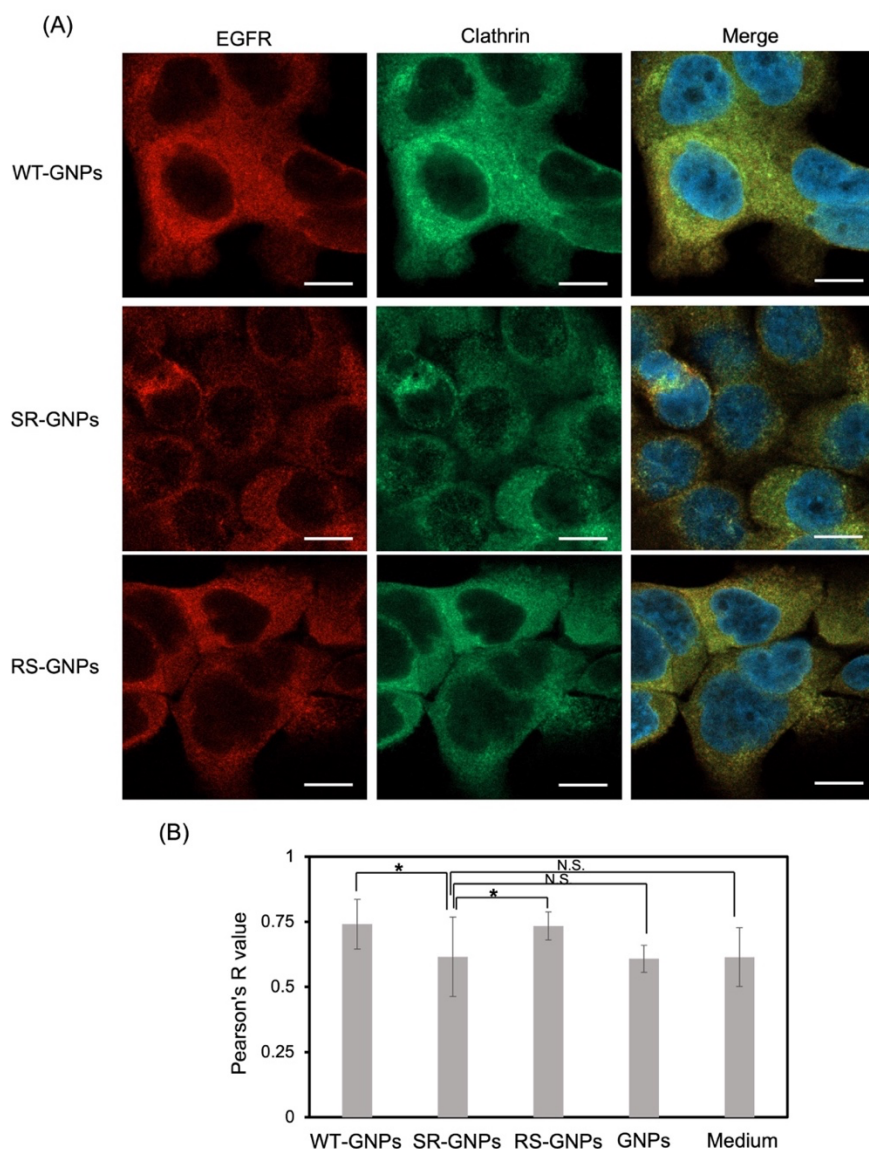


Figure 4-4 Analysis of clathrin-EGFR colocalization after EGF-GNPs stimulation. (A) Confocal microscopy images of clathrin (green) and EGFR (red), as well as merged images of the channels together with nuclear stain in blue. A431 cells were treated with EGF-GNPs at 6 nM for 3 h, followed by immunostaining. Medium: A431 cells were solely exposed to a culture media devoid of GNPs or EGF-GNPs. Scale bar: 10 μ m. (B) The degree of clathrin and EGFR colocalization was quantified based on Pearson's R-value. Each condition had 13–19 cells that assessed statistical differences. The data reflects the mean and standard deviation among tested cells. A significant difference from SR-GNPs was examined using the student's *t*-test ($P < 0.05$ (*)). Reproduced from with Ref. [2] permission from Springer Nature, Copyright [2023].

4.5 Discussion

The manipulation of physicochemical properties of EGF-NPs, such as EGF density and particle size, has been examined to boost therapeutic effectiveness by

considering the alternated interaction of the EGF-NPs and cells[10–12]. However, no studies have explored the effects of the biological properties of EGF mutants and the orientation of EGF to NPs on EGF-GNPs-induced cytotoxicity. Given this, in the last chapters, two lysine-free EGF mutants (RS and SR) were created to confine the conjugation site to the *N*-terminus of the EGF, which exhibited different cytotoxicity. Further investigation was needed to determine how the synergistic effect of the mutant-derived activity alteration of the EGF molecule and the orientation affect the cytotoxic induction of EGF-GNPs. By considering earlier understanding in the postulated mechanisms of induced cytotoxicity with EGF-NPs, including EGFR activation[11], EGF-GNPs uptake[10], and endocytic trafficking of EGF-GNPs and EGFR[5], I conducted in-detail experiments to address these possibilities to clarify the major reason for the diveresed responses among EGF-GNPs based on lysine-free mutants. First, I studied the EGFR activation state after treatment with various EGF-GNPs by an antibody array (Figure 4-1). The results showed that different EGF variants (WT, SR, and RS)-conjugated GNPs induced identical phosphorylation patterns. Meanwhile, the quantified phosphorylation levels of the three main phosphorylation sites of EGFR were also verified, which revealed no significant difference between various EGF-GNPs (Figure 4-2). Of note, the EGFR expression levels of the cells after treatment with the multiple EGF-GNPs were comparable, indicating it was not the reason for the lack of significant difference in the phosphorylation level between various EGF-GNPs. These results suggest that, at least under the circumstances of this experiment, the cytotoxic capabilities various EGF-GNPs were not correlated with the activated state of EGFR. As a result, certain other elements should contribute to the potent cytotoxicity of SR-GNPs. Then, cellular uptake of the EGF-GNPs by using A431 cells was investigated. The obtained ranking of various EGF-GNPs was ordered as follows: RS-GNPs > SR-GNPs > WT-GNPs (Figure 4-3). This trend is consistent with the binding activities of various EGF-GNPs (Figure 3-5), which makes sense given that cells tend to take up higher affinity nanoparticles more readily[13]. It also suggests that the

binding activities of these different kinds of EGF-GNPs evaluated by SPR are trustworthy and related to their activities to EGFR in cell membranes. It should be emphasized, nevertheless, that the trends in binding activities and cellular uptake are different from the tendency in the potential of EGF-GNPs to cytotoxic induction: SR-GNPs > RS-GNPs > WT-GNPs. Therefore, the amount of uptaken EGF-GNPs might not be the reason for the selectively increased cytotoxicity of SR-GNPs. Then, in order to explore the mechanism behind the inverse ordering between cytotoxicity and binding activities, I employed immunostaining to identify the reason for the enhanced cytotoxicity of endocytic trafficking routes. The lower value of the colocalization index of SR-GNPs suggested that they were internalized to the cells via the clathrin-independent endocytosis, at least partially (Figure 4-4). In contrast, RS-GNPs and WT-GNPs mainly took the clathrin-dependent route. Meanwhile, the kinetics of clathrin-mediated endocytosis are widely known to be faster than those of clathrin-independent endocytosis[7,14]. In addition, another study discovered that a lesser capability of EGF to induce apoptosis was linked to a greater incidence of EGFR endocytosis[15]. More specifically, an early work in my group reported that the unique triggering of apoptosis by EGF-GNPs was accomplished by converting the endocytosis route from a clathrin-mediated route to a caveolin-dependent (clathrin-independent) route upon conjugating soluble EGF to GNPs[5]. Based on the findings in this thesis and other papers, I infer that selective engagement of the clathrin-independent route is more critical for SR-GNPs to induce more apoptosis than RS-GNPs and WT-GNPs.

Nonetheless, further research is necessary to thoroughly understand the changes in endocytosis pathways of SR-GNPs. By varying different parameters, such as surface nanoparticle surface charges[6] and ligand densities[7], similar alterations in the endocytotic trafficking have also been seen for the NPs which were functionalized with biological ligands or chemical ligands. In each scenario, it was seen that the increased overall affinities of the NPs with cells resulted in a transition from clathrin-independent to the clathrin-dependent route. In my system, the charges of the EGF-GNPs were

almost the same between different EGF variant conjugates, which might not be the reason for the switched endocytic pathway. However, these findings are in line with the different endocytosis routes, which I noticed for RS-GNPs and SR-GNPs, given the fact that RS-GNPs have higher binding activity than SR-GNPs. The clathrin-dependent endocytosis pathway, which is the route that soluble EGF initially travels, might be restored in the case of WT-GNPs (less than 8 EGF/GNP, see last chapter). This is because the multivalent character of the EGF-GNPs was vanished presumably due to reduced functional EGF ligands on the GNP surface, returning to the endocytosis route to the clathrin-dependent pathway. Except that, I cannot completely rule out the idea that SR-EGF has evolved a unique intrinsic role in initiating EGFR to the clathrin-independent route.

4.6 Conclusion

This study demonstrated how the EGFR interacted differentially with GNPs conjugates, which employed different EGF variants (wild-type EGF and lysine-free EGF mutants (SR and RS), leading to other features of downstream processes such as EGFR activation, cellular uptake, and EGFR endocytic trafficking. Eventually, the preferentially activated clathrin-independent route was the potential for the increased cytotoxicity induction of SR-GNPs, which originated from the controlled orientation and appropriate binding affinity of the SR compared with WT and RS, highlighting the significance of EGFR trafficking in the improvement of the anti-cancer effect of EGF-GNPs. Additionally, a potent high cellular uptake of RS-GNP is promising for other EGFR-targeted cancer therapies.

Reference

- 1 Jorissen, R. N., Walker, F., Pouliot, N., Garrett, T. P. J., Ward, C. W. and Burgess, A. W. (2003) Epidermal growth factor receptor: mechanisms of activation and signalling. *Exp. Cell Res.* **284**, 31–53.
- 2 Zhang, A., Abdellatef, S. A. and Nakanishi, J. (2023) Mechanistic investigation into selective cytotoxic activities of gold nanoparticles functionalized with epidermal growth factor variants. *Anal. Sci.* **39**, 395–405.
- 3 Zhang, Q. and Reinhard, B. M. (2018) Ligand density and nanoparticle clustering cooperate in the multivalent amplification of epidermal growth factor receptor activation. *ACS Nano* **12**, 10473–10485.
- 4 Wu, L., Xu, F. and Reinhard, B. M. (2016) Nanoconjugation prolongs endosomal signaling of the epidermal growth factor receptor and enhances apoptosis. *Nanoscale* **8**, 13755–13768.
- 5 Yamamoto, S., Iwamaru, Y., Shimizu, Y., Ueda, Y., Sato, M., Yamaguchi, K. and Nakanishi, J. (2019) Epidermal growth factor-nanoparticle conjugates change the activity from anti-apoptotic to pro-apoptotic at membrane rafts. *Acta Biomater.* **88**, 383–391.
- 6 Chakraborty, A. and Jana, N. R. (2015) Clathrin to lipid raft-endocytosis via controlled surface chemistry and efficient perinuclear targeting of nanoparticle. *J. Phys. Chem. Lett.* **6**, 3688–3697.
- 7 Dalal, C., Saha, A. and Jana, N. R. (2016) Nanoparticle multivalency directed shifting of cellular uptake mechanism. *J. Phys. Chem. C* **120**, 6778–6786.
- 8 Pearson, K. (1896) Mathematical contributions to the theory of evolution. III. regression, heredity and panmixia. *Philos. Trans. R. Soc. London* **187**, 253–318.
- 9 Manders, E. M. M., Stap, J., Brakenhoff, G. J., Van Driel, R. and Aten, J. A. (1992) Dynamics of three-dimensional replication patterns during the S-phase,

-
- analysed by double labelling of DNA and confocal microscopy. *J. Cell Sci.* **103**, 857–862.
- 10 Yasami-Khiabani, S., Karkhaneh, A., Shokrgozar, M. A., Amanzadeh, A. and Golkar, M. (2020) Size effect of human epidermal growth factor-conjugated polystyrene particles on cell proliferation. *Biomater. Sci.* **8**, 4832–4840.
 - 11 Yamamoto, S. and Nakanishi, J. (2021) Epidermal growth nanoparticle conjugates-induced cellular responses : Effect of interfacial parameters between cell and nanoparticle. *Anal. Sci.* **37**, 741–745.
 - 12 Khanehzar, A., Fraire, J. C., Xi, M., Feizpour, A., Xu, F., Wu, L., Coronado, E. A. and Reinhard, B. M. (2018) Nanoparticle-cell interactions induced apoptosis: A case study with nanoconjugated epidermal growth factor. *Nanoscale* **10**, 6712–6723.
 - 13 Bazak, R., Hourri, M., Achy, S. El, Kamel, S. and Refaat, T. (2016) Cancer active targeting by nanoparticles: a comprehensive review of literature. *J Cancer Res Clin Oncol.* **141**, 769–784.
 - 14 Rejman, J., Bragonzi, A. and Conese, M. (2005) Role of clathrin- and caveolae-mediated endocytosis in gene transfer mediated by lipo- and polyplexes. *Mol. Ther.* **12**, 468–474.
 - 15 Rush, J. S., Quinalty, L. M., Engelman, L., Sherry, D. M. and Ceresa, B. P. (2012) Endosomal accumulation of the activated epidermal growth factor receptor (EGFR) induces apoptosis. *J. Biol. Chem.* **287**, 712–722.

Chapter 5

Conclusive remarks and prospects

5.1 Conclusions

Traditional cancer therapies, such as chemotherapy, have successfully treated many cancers but are restricted by undesirable side effects. As a result, the creation of a novel cancer treatment approach is required. Meanwhile, many studies demonstrate that the membrane receptor, epidermal growth factor receptor (EGFR), is frequently overexpressed in tumor cells and facilitates tumor formation. Given this, selective suppression of EGFR signaling is being evaluated as a possible cancer therapeutic strategy. Based on this, several EGFR-targeted inhibitors have been discovered and show effective anticancer effects. However, it is difficult to treat cancer entirely due to the developed resistance. As a result, creating a novel cancer therapy modality is required.

Chapter 1 introduced the above-mentioned current situation of cancer therapy, specifically EGFR-targeted anti-cancer agents, and discussed the importance of developing a new modality for cancer therapy. As an alternative, EGF-NPs was introduced to have significant advantages over the conventional ones but still needs to improve their existing limitation regarding insufficient cytotoxic activity against tumor cells. Then, the possible reason for the low activity and the promising strategy based on lysine-free mutants to overcome were proposed. Finally, I hypothesized that the GNP conjugates of the lysine-free EGF mutants would exhibit improved cytotoxic activity through orientation control as well as changing intrinsic activity of EGF ligands and further elucidate the design rationale for the development of more potent EGF-

GNPs.

Chapter 2 introduced the significance of the choice of substituted amino acids at lysine residues based on the crystal structure of the EGF-EGFR complex. Based on this, two new lysine-free EGF mutants (K28S/K48R (SR); K28R/K48S (RS)) were designed, prepared, and purified. Finally, together with wild-type (WT) EGF, the activities of these EGF variants were evaluated. The results confirmed that the lysine-free EGF was successfully developed and retained bioactivity and binding affinity to EGFR compared with WT EGF, which is suitable for the following study for the preparation of the site-specific conjugates to investigate the effect of the orientation to the EGF-GNPs. Additionally, EGF mutants are ideal as model proteins to examine the consequences of mutation to EGF-GNPs due to their somewhat altered features.

Chapter 3 characterized the lysine-free EGF-conjugated gold nanoparticles (GNPs). Combined with the results in chapter 2, the successful control of the EGF mutants on the GNP surface was confirmed. The biological assays demonstrated an enhanced and no different cytotoxicity in cancer cells for SR-GNPs and RS-GNPs, respectively, compared to WT-GNPs. This further verified the development of lysine-free EGF mutants as a useful strategy to improve the activity of EGF-GNPs. At the same time, it identified an inconsistent relationship between binding activity and cytotoxic activity between SR-GNPs and RS-GNPs, indicating a synergistic effect of orientation control and properties of the mutants themselves in the induction of the cytotoxic effect on cancer cells.

Chapter 4 investigated the mechanism of cytotoxic induction by EGF-GNPs using different EGF mutants to elucidate the inconsistency in the activities of the mutant EGF-GNPs identified in chapter 3. The analysis of cellular responses to various EGF-GNPs indicated that, rather than EGFR phosphorylation or the uptake of nanoconjugates, selective activation of the clathrin-independent pathway was critical to induce higher cytotoxic activities in the SR-GNPs over RS-GNPs and WT-GNPs.

This is an important finding in the molecular mechanisms of unique cytotoxic activities of EGF-GNPs. Also, it sheds light on the significance of endocytosis pathways in the design rationale of anti-cancer EGF-GNPs.

In conclusion, the lysine-free EGF mutants, which were used to conjugate the EGF to GNP at a site-specific orientation, can influence the cytotoxic induction of the EGF-GNPs to a different degree, which verified my hypothesis. In addition, further mechanistic investigation of SR-GNPs and RS-GNPs confirmed how the properties of the EGF mutant influenced the cytotoxic induction of the EGF-GNPs. More specifically, it sheds light on the significance of the selective activation of the clathrin-independent endocytotic pathway in the cytotoxic activity of EGF-GNP, providing useful information for further related studies for the design and optimization of the protein conjugates to obtain the improved anticancer effect.

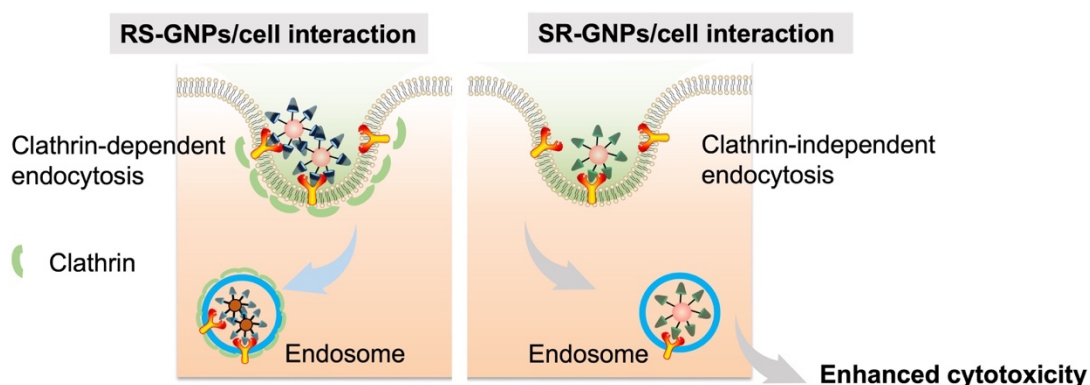


Figure 5-1 Illustration of the conclusion of this work. Two lysine-free EGF mutants were created to develop site-specifically orientated GNPs conjugates. The EGF mutants conjugated GNPs show different levels of the cytotoxic induction with selective activation of the endocytic pathway, providing useful information in the design rationale of anti-cancer EGF-GNPs. Reproduced from with Ref. [1] permission from Springer Nature, Copyright [2023].

5.2 Future Perspectives

In this work, the SR-GNPs demonstrated enhanced cytotoxicity to the cancer cells. However, the work is investigated in vitro. As the candidate for anticancer drugs, it is necessary to apply EGF-GNPs in vivo since there are many differences between in vitro and in vivo, such as the physical conditions and pharmacokinetics. All these factors can influence the outcome of the drug efficacy, which is also the main issue in anticancer drug development. Given this consideration, in the future, the SR-GNPs can be applied in vivo to investigate the cytotoxicity of living tumors.

In addition, given the advantages of designed lysine-free EGF, SR, and RS can be used as orientation-controlled ligands and combined with other cancer therapy to take advantage of their potentially high targeting efficiency. For example, traditional phototherapy is limited by non-selectivity, which can also kill normal cells[2,3]. The designed lysine-free EGF variants can be conjugated to the nanoparticles, such as gold nanorod, a commonly used nanoparticle for photothermal therapy due to their excellent electronic and optical properties[4]. The EGF conjugates will selectively accumulate in the tumor cell, overexpressing EGFR. In addition, the cytotoxicity of the EGF conjugates themselves could also enhance the outcome of photothermal therapy. Based on this, the developed EGF variants was expected to apply to this strategy to reduce the side effect to the normal cells and the dosage used for cancer treatment.

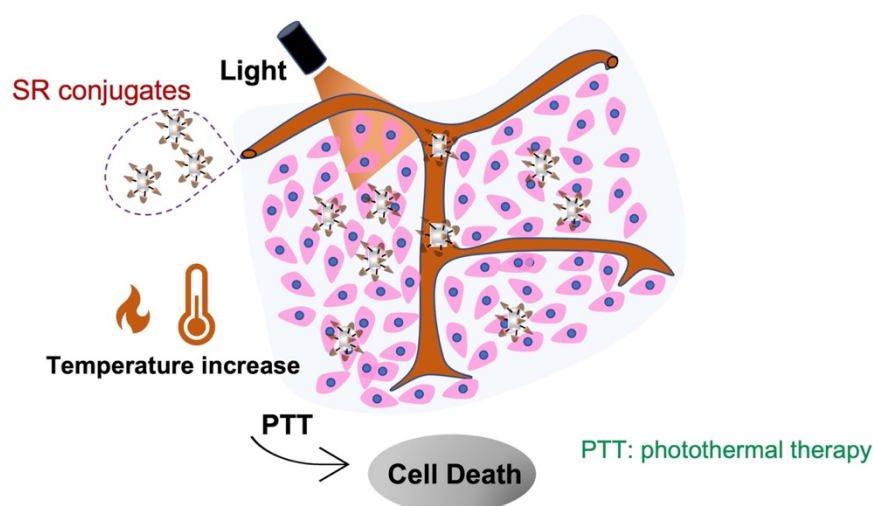


Figure 5-2 Illustration of the possible application of mutant EGF.

Reference

- 1 Zhang, A., Abdellatef, S. A. and Nakanishi, J. (2023) Mechanistic investigation into selective cytotoxic activities of gold nanoparticles functionalized with epidermal growth factor variants. *Anal. Sci.* **39**: 395-405.
- 2 Zhang, S. J., Jia, N. Y., Shao, P., Tong, Q., Xie, X. Q. and Bai, M. F. (2014) Target-selective phototherapy using a ligand-based photosensitizer for Type 2 cannabinoid receptor. *Chem. Biol.* **21**, 338–344.
- 3 Tong, R. and Kohane, D. S. (2012) Shedding light on nanomedicine. *Wiley Interdiscip Rev Nanomed Nanobiotechnol.* **4**, 638–662.
- 4 Bansal, S. A., Kumar, V., Karimi, J., Singh, A. P. and Kumar, S. (2020) Role of gold nanoparticles in advanced biomedical applications. *Nanoscale Adv.* **2**, 3764–3787.

Acknowledgment

At the end of this thesis, here, I first would like to express my sincere gratitude to my supervisor Prof. Jun Nakanishi, the group leader of Mechanobiology Group, Research Center for Functional Materials, National Institute for Materials Science (NIMS), and also the Professor of Dept. Nanoscience and Nanoengineering, Waseda University. I appreciate his careful guidance, enlightening discussion, and genuine encouragement of my research. From him, I learned how to face failure and solve problems. Thank him for his care, understanding, and support in my life. Next, I would like to thank my thesis committee members: Prof. Akiyoshi Taniguchi, Prof. Takashi Tanii, and Prof. Naoya Takeda. I would like to express my gratitude for their helpful advice and insightful comments.

I would like to thank Dr. Shimaa A. Abdellatef, a very kind and warm person who gave me a lot of guidance and help. Also, thank her for the prayers she gave me when I struggled. I would like to thank Dr. Shota Yamamoto for his help with my experiments and thesis. I also would like to thank Dr. Kenji Sugiyama, who took me to the genetic recombination field and much help for my research. I would like to express my gratitude to Dr. Chia-jung Chang for her support in my research and living.

I also would like to thank all members of the Mechanobiology Group, Ms. Junhong Zhou, Dr. Hongxin Wang, Dr. Zhou Lu, Mr. Kazuhiko Tatematsu, Mr. Yuji Kamiyama, Dr. Chiaki Yoshikawa, Prof. Takeshi Ueki, and Ms. Aya Saruwatari, for their support and help with my research.

Finally, I would like to thank my family members for their endless love and patience with me. Thank them for their understanding and support. I also would like to thank my friends in Japan and China for making my life more colorful.

ZHANG Aiwen
Japan, February 2023

List of research achievements

1. ○ Zhang, A., and Nakanishi, J. (2021) Improved anti-cancer effect of epidermal growth factor-gold nanoparticle conjugates by protein orientation through site-specific mutagenesis. *Sci. Technol. Adv. Mater.*, **22**, 616–626.
2. ○ Zhang, A., Abdellatef, S. A. and Nakanishi, J. (2023) Mechanistic investigation into selective cytotoxic activities of gold nanoparticles functionalized with epidermal growth factor variants. *Anal. Sci.* **39**: 395-405.
3. Zhang, A., Tao, G., and Wang, J. (2018) Assembly of bioconjugated rod-nanotags and multilayer plasmonic nanorod-array for ultrasensitive SERS detection of *S. aureus* bacteria. *J. Nanoparticle Res.*, **20**, 97.
4. Qiu, L., Wang, W., Zhang, A., Zhang, N., Lemma, T., Ge, H., Toppari, J. J., Hytönen, V. P. and Wang, J. (2016) Core-shell nanorod columnar array combined with gold nanoplate-nanosphere assemblies enable powerful in situ SERS detection of bacteria. *ACS Appl. Mater. Interfaces*, **8**, 24394–24403. (co-first author)
5. Wang, W., Hynninen, V., Qiu, L., Zhang, A., Lemma, T., Zhang, N. Ge, H., Toppari, J. J., Hytönen, V. P. and Wang, J. (2017) Synergistic enhancement via plasmonic nanoplate-bacteria-nanorod supercrystals for highly efficient SERS sensing of food-borne bacteria. *Sensors Actuators, B Chem.*, **239**, 515–525.